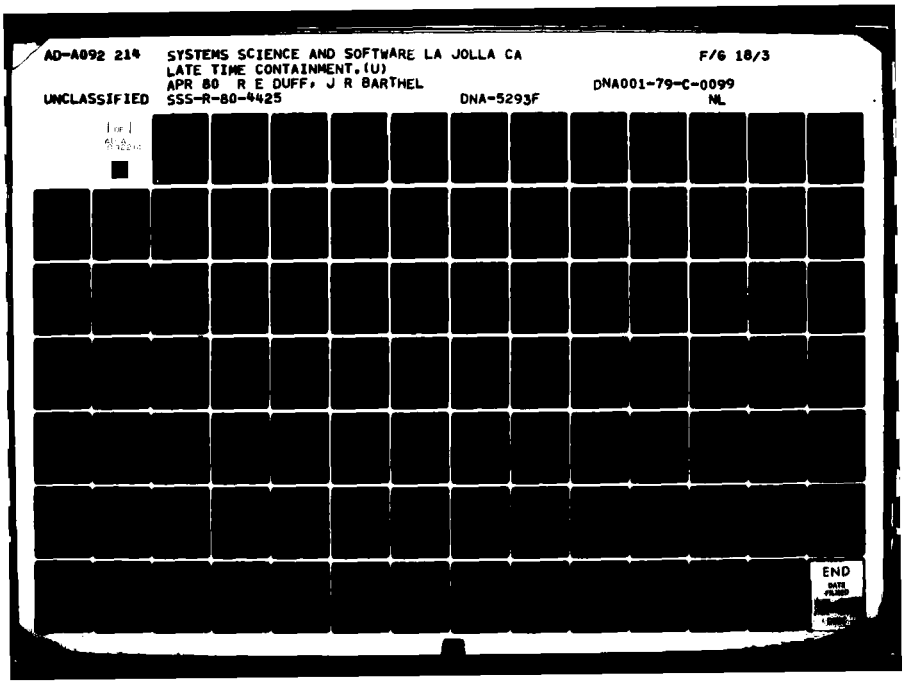
AD-A092 214
SYSTEMS SCIENCE AND SOFTWARE LA JOLLA CA
F/G 18/3
LATE TIME CONTAINMENT,(U)
APR 80 R E DUFF, J R BARTHEL
DNA001-79-C-0099
UNCLASSIFIED
SSS-R-80-4425
DNA-5293F
NL
END

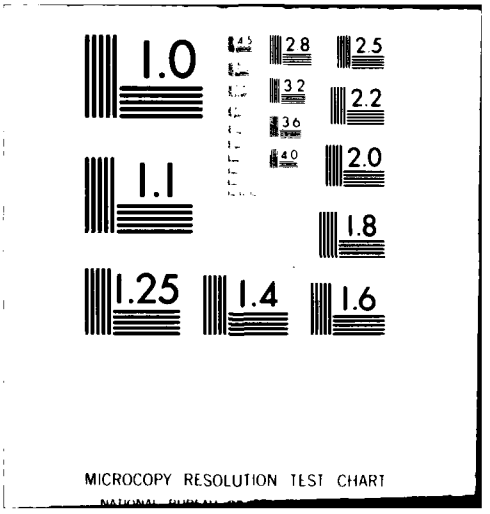
1.0
1.1
1.25
1.4
1.6
1.8
2.0
2.2
2.5
2.8
3.2
3.6
4.0
MICROCOPY RESOLUTION TEST CHART

DNA 5293F

LATE TIME CONTAINMENT

Systems, Science and Software
P.O. Box 1620
La Jolla, California 92038

18 April 1980

Final Report for Period 1 January 1979—31 December 1979

CONTRACT No. DNA 001-79-C-0099

APPROVED FOR PUBLIC RELEASE;
DISTRIBUTION UNLIMITED.

THIS WORK SPONSORED BY THE DEFENSE NUCLEAR AGENCY
UNDER RDT&E RMSS CODE B345079462 J24AAXYX98366 H2590D.

Prepared for
Director
DEFENSE NUCLEAR AGENCY
Washington, D. C. 20305

Destroy this report when it is no longer needed. Do not return to sender.

PLEASE NOTIFY THE DEFENSE NUCLEAR AGENCY, ATTN: STTI, WASHINGTON, D.C. 20305, IF YOUR ADDRESS IS INCORRECT, IF YOU WISH TO BE DELETED FROM THE DISTRIBUTION LIST, OR IF THE ADDRESSEE IS NO LONGER EMPLOYED BY YOUR ORGANIZATION.

UNCLASSIFIED

SECURITY CLASSIFICATION OF THIS PAGE (When Data Entered)

(19) REPORT DOCUMENTATION PAGE	READ INSTRUCTIONS BEFORE COMPLETING FORM
(18) REPORT NUMBER: DNA 5293F	2. GOVT ACCESSION NO.: AD-A092214	3. RECIPIENT'S CATALOG NUMBER:
(6) 4. TITLE (and Subtitle): LATE TIME CONTAINMENT,	(9) 5. TYPE OF REPORT & PERIOD COVERED: FINAL REPORT, 1 Jan [illegible]—31 Dec 79
	(14) 6. PERFORMING ORG. REPORT NUMBER: SSS-R-80-4425
(10) 7. AUTHOR(s): R. E. Duff, J. R. Barthel	(17) X983	(15) 8. CONTRACT OR GRANT NUMBER(s): DNA 001-79-C-0099
9. PERFORMING ORGANIZATION NAME AND ADDRESS: Systems, Science and Software, P.O. Box 1620, La Jolla, California 92038	10. PROGRAM ELEMENT, PROJECT, TASK AREA & WORK UNIT NUMBERS: (16) SUBTASK J24AAXYX983-66
11. CONTROLLING OFFICE NAME AND ADDRESS: Director, Defense Nuclear Agency, Washington, D.C. 20305	(11) 12. REPORT DATE: 18 Apr [illegible]80; 13. NUMBER OF PAGES: 96
14. MONITORING AGENCY NAME & ADDRESS (if different from Controlling Office)	(12) 45	15. SECURITY CLASS. (of this report): UNCLASSIFIED
	15a. DECLASSIFICATION/DOWNGRADING SCHEDULE

16. DISTRIBUTION STATEMENT (of this Report)

Approved for public release; distribution unlimited.

17. DISTRIBUTION STATEMENT (of the abstract entered in Block 20, if different from Report)

18. SUPPLEMENTARY NOTES

This work sponsored by the Defense Nuclear Agency under RDT&E RMSS Code B345079462 J24AAXYX98366 H2590D.

19. KEY WORDS (Continue on reverse side if necessary and identify by block number)

Residual stress
Grout spheres
Cavity pressures
LOS flow

20. ABSTRACT (Continue on reverse side if necessary and identify by block number)

Major contributions in the Late Time Containment research effort are summarized. Test design activity showed that cavity venting into a tunnel could effectively lower cavity pressure on a fast time scale and that a reasonable, fast-turn-around horizontal line of sight system could be developed for satellite testing. Analysis of past experience has led to a containment summary report for Mighty Epic and much of the data for a Diablo Hawk report. A study of cavity pressure measurements confirms

DD FORM 1 JAN 73 1473 EDITION OF 1 NOV 65 IS OBSOLETE

UNCLASSIFIED

SECURITY CLASSIFICATION OF THIS PAGE (When Data Entered)

388507

20. ABSTRACT (Continued)

that complex processes are involved probably including some form of cavity gas leakage at late time. LOS flow modeling and calculations based on new techniques are in reasonable agreement with the limited data available. Flow calculations of PI test configurations probably indicate that the neglect of the pipe wall in the calculations was detrimental. An analysis of grout sphere experiments by SRII shows that strong evidence for rapid stress relaxation exists in the data. Finally, several miscellaneous activities are detailed.

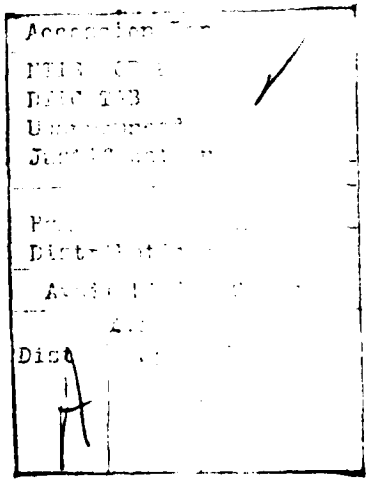

TABLE OF CONTENTS

Section		Page
1	INTRODUCTION	7
2	TEST DESIGN CONTRIBUTIONS	8
2.1	CAVITY VENTING FOR LOW-YIELD TEST DESIGN	8
2.2	SATELLITE TESTING CONCEPT	10
3	ANALYSIS OF EXPERIENCE	12
3.1	MIGHTY EPIC CONTAINMENT SUMMARY REPORT	12
3.2	DIABLO HAWK	14
3.3	CAVITY PRESSURE	15
4	LOS FLOW ANALYSIS	18
5	LOS ENERGY FLOW SIMULATION	23
5.1	SUMMARY OF EXPERIMENTAL RESULTS	23
5.2	CALCULATIONAL STUDIES OF SYMMETRIC CONFIGURATIONS	30
5.3	A SCENARIO FOR THE PERFORMANCE OF THE SYMMETRIC CONFIGURATIONS	44
5.4	CALCULATIONAL STUDIES OF ASYMMETRIC CONFIGURATIONS	50
5.5	IMPLICATIONS FOR UNDERGROUND NUCLEAR TESTS	54
6	SRII GROUT SPHERE PROGRAM CONTRIBUTIONS	59
6.1	ANALYSIS OF EXPERIMENTAL DATA	59
6.1.1	Comparison of 2C4 Pressurization and Residual Stress Relaxation	59
6.1.2	Cavity Filling	67
6.1.3	LD2C4 Experiments	79
6.1.4	Summary	81
6.2	EXPLOSION CALCULATIONS	82

TABLE OF CONTENTS (Continued)

Section		Page
7	MISCELLANEOUS TASKS	86
7.1	CEP SUPPORT	86
7.2	SLIFER STUDIES	86
7.3	SWIS CODE DEVELOPMENTS	87
7.4	STREAK/UNION IMPROVEMENTS	87
8	REFERENCES	89

LIST OF ILLUSTRATIONS

Figure		Page
5.1	Configuration of the APC-1, 2 Explosive Driver Experiments	24
5.2	Configuration of the LS-II Experiment	25
5.3	Postulated Standard Distribution of Hole Volumes for Standard LS Cases	31
5.4	Configuration of imploded pipe driven by nitromethane at 1.65 μsec in a calculation using the vaporization-condensation model	33
5.5	Calculated pressure at aluminum target plate, APC-1, 2	34
5.6	Energy evolution in vapor and condensate jet for LS calculations	37
5.7	Evolution of Material boundaries in the PI "Standard LS" Case	38
5.8	Evolution of material boundaries in the calculation of the "Lead Wrap" case	40
5.9	Evolution of material boundaries in the calculation of the PI "12 inch Standoff" case	43
5.10	Symmetric liner jetting geometry	46
5.11	Time sequence from 2-D planar calculations of asymmetric collapse. Materials: 1 steel, 2 = wet sand, 3 = lead, 4 = polyolefin	51

LIST OF ILLUSTRATIONS (Continued)

Figure		Page
6.1	Pressure injected volume relation at first minimum for 2C4 grout spheres	62
6.2	Relation between minimum cavity pressure and fracture initiation pressure. The experiments indicated with ● all contained faults, interfaces or tunnels	64
6.3	Fracture initiation pressure as a function of fracture time for 2C4 unvented grout spheres	65
6.4	Grout spheres hydrofracture data summary	66
6.5	Calculated residual stress relaxation as a function of time and fracture initiation pressure for 2C4 grout spheres	68
6.6	Calculated and measured pressure decay in exploded grout sphere	69
6.7	Grout sphere cavity pressure decay resulting from water intrusion	71
6.8	Original and compliance-corrected pressurization records for tests 169 and 170	74
6.9	Compliance curve for SRII hydrofracture system	75
6.10	Comparison of compliance corrected and calculated pressurization records for unvented 2C4 grout spheres	78
6.11	Hydrofracture pressures for unvented exploded cavity tests 159, 170, 189, 215, and 216 - material property	80

LIST OF TABLES

Table		Page
5.1	Summary of Physics International Co.'s APC Experiment Series	27
5.2	Summary of Physics International Co.'s LOS simulation experiment series	28
5.3	Liner mass per unit length for symmetric LS configurations and comparison with hole volumes in witness plates	47
6.1	Selected data from 2C4 unvented grout sphere pressurizations	61
6.2	Calculated pressure-volume relationship for unvented 2C4 grout sphere tests	77

SECTION 1
INTRODUCTION

This annual report describes those tasks which have been considered during this contract year. The Late Time Containment research effort is a continuing program to understand the phenomenology and insure the safe containment of underground nuclear explosions and to assist Defense Nuclear Agency (DNA) in the preparation of designs for such tests. Some of the tasks discussed were begun in prior years. Some of the subjects are still underway.

It is a well established policy to publish topical reports from time to time which fully describe work done in a particular technical area. Therefore, overall summary reports such as this are relatively limited documents which are designed to provide the interested reader with a good overview of the tasks undertaken and with the significance of the results obtained. This report is not intended as an exhaustive presentation of each subject area except in the PI and SRII experimental areas which are of particular interest to the community and topical reports are not yet timely. For extended discussion in other areas the reader is referred to the appropriate topical reports which have been or will be widely distributed within the containment community.

This report will document efforts in a number of areas. Contributions made to the development of low-yield test designs, both considered singly and as a technique for repetitive satellite testing, will be described. Considerable analysis of past experience has been accomplished and will be reported. The development of understanding of LOS flows will be discussed. Emphasis will be placed on the design and analysis of continuing test programs underway at Physics International and SRI International (SRII). In the latter case, it is significant to emphasize the influence of fluid diffusion on residual stress field relaxation. In addition, a number of miscellaneous projects will be discussed.

SECTION 2
TEST DESIGN CONTRIBUTIONS

During this year two aspects of low-yield tests have been studied. The first investigates the effect of cavity venting on late-time cavity pressure for a low-yield test. The objective is to clarify the potential benefits to be derived from a deliberate venting system to reduce the late-time cavity pressure from such tests.

The second is a horizontal, low-yield test configuration designed so that repetitive use of the hardware is practical. This would provide an economical, fast turn-around system for satellite testing.

2.1 CAVITY VENTING FOR LOW-YIELD TEST DESIGN

A report by Bailey and Duff (Reference 1) summarizes the work accomplished in this area. Two calculations were done for 160 T devices. In one case, a conventionally tamped shot was assumed; in the other an infinitely long three meter diameter tunnel was assumed available as a dump volume. This tunnel was separated from the zero room by a 1 m hickness of tuff. The two calculations were run until the free field ground shock pressure had fallen to the order of 500 MPa at which point the numerical results were becoming noisy.

Three questions were asked at the outset of the investigation. These questions and the answers obtained will be repeated in the following paragraphs.

- Can a vent system of this sort significantly reduce cavity pressure and reduce the threat to the stemming plug?

This can be best answered by determining the rate at which energy is escaping from the zero room and comparing that rate with others

of interest. It was shown that the internal energy of the flowing gas in the tunnel was about 9×10^{10} ergs/gm everywhere. This, plus calculated values of density and flow velocity leads to a total energy flux up the tunnel of about 1.2×10^{20} erg/sec. The total yield of the explosion was 6.7×10^{18} ergs. Therefore, if the process proceeded at a steady rate (which of course it will not) all of the device energy would be vented from the cavity in 56 msec. Since only about one-third of the explosion energy usually remains in the cavity, the available energy would be vented in about 20 msec. This calculation is certainly not correct in detail, but it does suggest that venting into a tunnel of this cross-section would significantly reduce cavity pressure on a time scale comparable with or shorter than that for cavity formation. The actual pressure history in the cavity and acting on the stemming plug at late time would depend on the total volume of vent tunnel available. Also friction and heat conduction losses would have important influences on that environment.

High pressure in the tunnels might represent a containment hazard through hydrofracture of the sort seen over the Red Hot and Deep Well drifts. This would need further investigation if the use of a vent tunnel were seriously contemplated.

- Would the ground shock which closes the LOS be degraded so that the stemming plug is shortened excessively?

The calculations provide an answer to this question. Because of the symmetry which was assumed in these calculations, the comparison of the radial shock amplitude provides the best indication, although it is admittedly an overestimate of the degradation to be expected. The shock amplitude is reduced only 12 percent at 4.6 msec by the vent tunnel. The shock location appears unchanged. We believe this to be a modest influence which would not have serious consequences for the stemming process. In fact, it might be advantageous to degrade the ground shock in the vicinity of the fast acting closure and the strong pipe beyond in the current low-yield test design.

- Will the vent tunnel be closed by the ground shock?

There is indication that the tunnel is starting to close at the end of the calculation. A similar tendency towards closure was seen in the Hybla Gold configuration. A simple flaring of the channel near the zero room fixed the problem in Hybla Gold, and the same alteration should be quite satisfactory for this application.

It appears to us that the late-time, high-pressure cavity environment in a low-yield test could be reduced significantly by the use of this venting scheme if that were judged necessary. Additional calculations to better define the late-time environment should be undertaken if interest is expressed in this possibility. In particular, the influence of finite tunnel length, heat conduction, diffusive losses, and possible tunnel hydrofracture all should be considered.

2.2 SATELLITE TESTING CONCEPT

At the request of Dr. C.P. Knowles, DNA headquarters, low-yield test configurations were sought which could provide economical, repetitive fluence for the testing of satellite systems. The concept which emerged from these studies and which was reported in a classified paper imagined that a straight tunnel 1.5 to 3 km long would be drilled from the portal into Rainier Mesa. The diameter at the portal end would be at least 3 m, and the satellite test chamber would be located at the tunnel portal. In other words, the vacuum system would run from the working point all the way to the outside world.

Since the pipe has a relatively small taper, closure in the immediate vicinity of the working point is easy to obtain using existing hardware.

It was contemplated that after each event, re-entry mining would push as close as possible to the original working point. Then a few

hundred feet of relatively small diameter LOS pipe would be replaced, a few closures such as a small taps and a fastgate would be rehabilitated and the facility could then be reused.

It was estimated that a facility with these characteristics could be constructed for approximately 20 million dollars exclusive of portal facilities, and that repeated use would cost 2 to 3 million dollars per shot. It was predicted that at least four shots per year could be obtained in a single facility.

This concept, and the cost estimates developed in connection with it, were a cooperative effort involving major contributions by Mr. LaComb and his staff at DNA Test Construction Branch, Mercury, Nevada.

SECTION 3
ANALYSIS OF EXPERIENCE

The analysis of experimental data and observations obtained on past events is a major source of understanding of containment phenomenology. During this past year, the containment summary report for the Mighty Epic event was completed and much of the preliminary work required for the Diablo Hawk containment summary report has been accomplished.

3.1 MIGHTY EPIC CONTAINMENT SUMMARY REPORT

The Mighty Epic document is a classified report based on the DNA nested containment vessel concept as was the original containment plan and presentation to the CEP. The various report sections follow this philosophy. They will be very briefly summarized in the following paragraphs.

An attempt was made to measure the residual stress generated by the explosion through hydrofracture measurements made near the cavity region after the event. Experimental difficulties were encountered, but hydrofracture pressure levels definitely increased because of the shot, and there is some evidence of stress decay over a period of a month or two after the event.

Two excellent records were obtained from slifers at 0.3 and 0.6 m from the LOS. These slifers run from the vicinity of the working point past the muffler. Well developed Brownlee knees are observed on both slifers, and a comparison of the slifer observations and UNION calculations suggests the slifer sensitivity level to be 0.14 GPa. This is slightly higher than the 0.1 GPa often quoted for this quantity.

The correlation of slifer shorting times in the region beyond the Brownlee knee shows that the crush signal comes from outside the LOS

and that extreme shock wave curvature occurs in the stemming near the LOS. The angle between the pipe axis and shock front at the pipe wall appears to be approximately 36 degrees.

The slifer records in the muffler region are peculiar in that large, discrete discontinuities occur in the records at several places. No satisfactory explanation for this behavior has been obtained, and a small investigation of the influence of various perturbations on slifer behavior has been conducted. It will be discussed at greater length in the Miscellaneous Tasks, Section 7 of this report.

Limited data were obtained from LOS pressure gages. These observed a fast plasma signal moving with a velocity of 16 km/sec which dissipates in the vicinity of the muffler. This is followed by a slower pulse moving at approximately 7.5 km/sec which reaches DAC-2 at approximately the time of DAC closure.

The slifer and LOS pressure gages indicate that a relatively modest plasma flow existed in Mighty Epic. This is interpreted as confirmation of the efficiency of the heavy tuballoy reversed cone used on this test.

On re-entry it was determined that grout motion of approximately 18 m occured in the vicinity of the muffler, the LOS was completely stemmed up to the DAC, and the DAC door was perforated to the lightening holes in several places but not seriously damaged.

Late-time gas seepage from the vicinity of the line of sight suggests that the CO observed is derived from carbonate minerals included in the desert fines used to make superlean grout, a major component of the stemming column.

The chimney has been studied by tracer gas techniques. It was found that gas seeps from the chimney to the paintbrush, however it does not leak to the surface or into the tunnel complex.

An interface experiment was made as part of a block motion investigation. It was observed that slippage of roughly 1 m occurred some distance above the paleozoic-tuff interface near the Mighty Epic explosion. The slippage occurred in a relatively weak, porous tuff bed. A number of other observations of block motion were obtained. The most notable was motion on fault 5 and on bedding plane 3bc. The Mighty Epic event was satisfactorily contained. Diagnostic efforts were more successful than in many previous tests, and analysis of the results has contributed to our understanding of explosion phenomenology.

3.2 DIABLO HAWK

Much of the information required for the preparation of the Diablo Hawk containment summary report has been collected and some analysis accomplished. The most instructive result to date has been the comparison of LOS flows in Diablo Hawk and Mighty Epic.

The system designs for these two events made use of massive tuballoy extensions. The Diablo Hawk design was thought to be an improvement over that of Mighty Epic. The slifer records of the two events, coupled with pressure measurements in the line of sight, suggest that the very fast plasma pulse in Diablo Hawk was less energetic than that observed in Mighty Epic. This is apparent because that pulse is not strong enough to crush the slifers and generate the familiar Brownlee knee configuration on the cable 0.6 m from the pipe.

On the other hand, the Diablo Hawk event showed a second gas pulse which was much more energetic than the second pulse observed in Mighty Epic. On Diablo Hawk this second pulse significantly distorts the slifer record, and it produces a reflected shock pressure at the closed DAC door of approximately 3 to 4 MPa (500 psi). No comparable pressure was observed in Mighty Epic. The second pulse on Diablo Hawk has been treated as a flow of steam presumably generated from the collapse of stemming material shortly beyond the end of the heavy extension. This is

attributed to the fact that the first pulse would cause less pipe expansion, and the ground shock-driven collapse would therefore occur faster and at greater pressure than in Mighty Epic. Excellent correlations between several observations have been developed.

The DAC-2 doors of Diablo Hawk were destroyed by the impact of stemming materials which occurred approximately one-half second after the explosion. The door fragments show signs of extensive high temperature erosion presumably related to the compression of the steam in the LOS by the oncoming stemming column.

3.3 CAVITY PRESSURE

A study (Reference 2) has been performed to evaluate the measured late time cavity pressure history. A knowledge of this history is important to pre-shot containment evaluation studies.

In recent years efforts have been made to calculate cavity pressure using material response codes. In these analyses a chemical equilibrium equation of state together with laboratory determined material strength data have been used to model tuff behavior. Assumptions inherent in the modeling and uncertainties in the true in situ material strength have led to large variations in predicted cavity pressure values. If these predictive models are to be used with confidence, it is imperative that they be calibrated and validated with measured cavity pressure data.

Recently, a number of apparently successful cavity pressure measurements have been obtained. Data acquisition began shortly after the cavity dynamic growth phase terminated and continued for many minutes during which time the pressure decayed significantly. These measurements are difficult to obtain because of the severe environment, and, as would be anticipated, there exist variations in recorded pressure values. Even though the measured initial cavity pressures fall within the uncertainty inherent in the predicted values, questions arise as to whether these data provide a true representation of the actual cavity pressure history.

Models describing the cavity gas pressure decay resulting from radiation-convection/conduction, spall, water intrusion, diffusion, and, leakage phenomena were studied. Evaluation of the late time pressure histories using these models indicate, assuming the measured data is viable and the initial predicted cavity gas thermodynamic state is reasonable, that

- Fundamentally different mechanisms are at least partially responsible for the observed pressure decay characteristics of the three cavities studied.

- No one single model, of those considered, is capable of reproducing all three measured pressure histories.

- With the exception of Hybla Gold, active time dependent physical changes must occur in order to produce features observed at very late times.

Pressure decay rates predicted using heat transfer or blow-off analyses are usually less than those measured. Cavity pressure histories can be modeled to some extent assuming water intrusion into the cavity or gas seepage (i.e., diffusion or leak) from the cavity. At very late times measured pressure decay rates in both the Diablo Hawk and LLL cavities were greater than predicted. Enhanced late time decay rates could be obtained if certain geometric features (i.e., leak path cross-section area, size or number of fractures penetrating the surrounding stress field, rate of surface degradation, and rate of cavity collapse, etc.) were allowed to change with time.

One or more of the phenomena investigated may be responsible for the cavity pressure decay observed following any given event. Since, in our opinion, these phenomena depend on details which, by their nature, cannot be modeled (i.e., exact cavity gas state, cavity gas mixing rates,

boundary layer effects, cavity surface uniformity, existence and thickness of melt layer, presence of fractures, fracture penetration depth, magnitude and uniformity of residual stress field, post-shot material characteristics, existence of flow paths, etc.) an all-inclusive model describing post-shot cavity pressure decay was not and cannot be presented.

Based on results determined from the predictive models, there is, however, little reason to believe the measured Diablo Hawk, Hybla Gold, and LLL cavity pressures are not representative of those existing immediately following the event. In that sense, it is of interest to note that the measured initial cavity pressures generally fall within the uncertainty inherent in the predicted values.

SECTION 4
LOS FLOW ANALYSIS

All previous studies have strongly indicated that wall ablation plays a key role in LOS flow. Consequently, there has been a continuing effort over a number of years to develop an adequate model of the ablation process for hydrodynamic calculations. During the past two years, a much more complete and defensible model of this process has evolved. Reference 3 contains a comprehensive description of this model and the results of many FLIP calculations performed with it.

The previous ablation model (Reference 4) was developed in 1974. The data base available at that time consisted of a limited number of LOS pressure histories, all of which were taken beyond the muffler; time of arrival data whose pressure threshold level was too uncertain for it to be very useful; and data from Physics International's explosive driven shock tubes (Reference 5). A major element of that modeling effort was a prior 2D calculational study of the effect of a muffler on LOS flow (Reference 6). That study concluded that the muffler did not have much influence on the arrival time and peak pressure at the DAC door and caused only a delay of the order of 20 percent in the time of the peak pressure. Therefore, LOS flow modeling at that time was based on the premise that slowing of the flow and pressure decay were due primarily to ablation and pipe expansion. It was found that an acceptable model would result if a low-energy process for removal of wall material, in addition to vaporization, were invoked. A complete model of the process of vaporization, melting, scouring of the melted layer, and condensation of vapor at the liquid surface, was then devised (Reference 4). This model contained an undetermined parameter, the scouring coefficient, which was the constant of proportionality in a postulated relationship between the local rate of scouring, the shear stress at the wall, and the liquid layer thickness. A value of this coefficient was found which led to good agreement between FLIP calculations

and the arrival data from the entire set of explosive shock tube experiments of Reference 5. The resulting model was then found to give results that were reasonably consistent with LOS data, considering the uncertainties in the data and the FLIP initial conditions as well as FLIP's inability to model 2D effects (Vol II of Reference 4). Subsequently, good agreement was obtained between data and calculations for LOS flow on the Hybla Fair event (Reference 7), which increased the level of confidence in the model.

Later, efforts to predict blast and shock propagation in MX buried trenches (under a separate DNA contract) led to the conclusion that a test dedicated primarily to careful measurement of ablation-dominated flow in air-filled pipes was needed. An extensive body of data was obtained on the subsequent Hybla Gold test. It was found that the vaporization/condensation/scour model of ablation did not give adequate agreement with this data. A model was then devised which took into account the influence of boundary layer growth behind the shock. The fact that fully developed turbulent flow does not occur until some distance behind the shock means that ablation products are not fully mixed in the flow immmediately behind the shock. A technique was devised to account properly for this. In addition, work which has become available in the literature since the earlier ablation modeling effort provides important results on the effect of ablation on heat transfer to the wall. The heat transfer rate is not independent of the ablation rate, and the availability of these specific results enabled us to develop an improved technique for determining the coupled heat transfer and wall ablation (vaporization) rates. The resulting model (Reference 3) produced reasonable overall agreement with all the available data from strong shock, ablation-dominated flows: Hybla Gold, Voitenko compressors, the "nuclear shock tube" event Marvel (Reference 8), and the PI shock tubes (Reference 5). Although some discrepancies remain, it is fair to say that the influence of wall ablation and boundary layer buildup on the shock attenuation process is reasonably well represented. Several anticipated refinements offer hope for even better agreement.

The new model does not invoke liquid scouring or include adjustable parameters - although some features, such as the representation of boundary layer closure and the transition to fully-developed turbulent flow, are somewhat uncertain and likely to remain so. The implication for LOS flow modeling is inescapable: liquid scouring does not appear to be necessary to explain any observed phenomenon, even in the PI shock tubes where the calculated stagnation enthalpy at long range becomes too low to cause wall vaporization. If this is true, it follows that the study described in Reference 6 greatly underestimated the effect of the muffler on LOS flow. It is not difficult to think of potentially important processes which that study could not address. For example, severe rupture of the muffler walls followed by deposition of much of the LOS vapor into the exposed grout either by porous flow or, more likely, condensation. Iron vapor should condense readily on a granular solid, especially when large cracks open up in such material.

The above conclusions were reached in early 1979. Between 1974 and that time significant LOS diagnostic data had been obtained between the working point and the muffler in Mighty Epic and Diablo Hawk. Hybla Fair, which had no muffler, also produced substantial data. These flows were recalculated using the new ablation model. The detailed results, which are given in Reference 9, make a good case for the new model. They are in better agreement with the data, in terms of times of arrival and peak pressures, than results obtained with the older model. The pulses calculated with either model are too long-lasting. It is argued that some attenuation mechanism that becomes important at a given point only long after the leading edge of the flow has passed is not accounted for in FLIP. Two mechanisms considered as strong candidates are: loss of vapor into cracks which open in the surrounding stemming after considerable pipe expansion occurs; and condensation of metal vapor on loose particulate matter in the vicinity of the advancing ground shock-driven pipe collapse.

This report also presents calculations of flow in the air-filled Diablo Hawk side pipe performed with the new ablation/boundary layer growth model. The results are consistent with the data. It is also argued, on the basis of the data, that the "low-threshold" slifer cables used in that pipe crush rather slowly in practice.

The Grove event, which has long been a puzzle because of the very slow LOS flow observed, is also discussed in detail in Reference 9. It is concluded that the measured pressure history obtained at the end of the pipe is due to ground shock, not vapor flow. The prompt vapor flow was evidently quite benign, which is attributed to the unusual configuration of Grove. Regions of CH_2 beads and Pb shot used in the close-in stemming had much larger air voids than stemming materials used in HLOS events. Furthermore, the sizes of the individual void spaces were quite large. Pipe ruptures exposing these media could lead to dramatic loss of LOS vapor.

Finally, an analysis of the proposed low-yield event, Dirtball, is given. It was found that even with a very fast-acting closure it may be necessary to employ a front-end design using tuballoy if adequate sample protection is to be assured.

The conclusions of the LOS flow studies carried out during the contract period may be summarized as follows:

- The new ablation model (Reference 3), in which there is no liquid scouring, is the most credible model of wall ablation now available.

- Mufflers may be much more effective in attenuating LOS flow than one would deduce from 2D muffler flow studies which ignore effects of rupture and of loss of vapor into the surrounding stemming.

- Some attenuation mechanism that is important at late time in LOS flow is missing from the calculational model. This may

be associated with a loss of LOS vapor either in the advancing pipe collapse process or into the surrounding stemming after large pipe expansion has occurred. The mechanism seems to have been particularly effective in the Grove event, which employed a plugged LOS and stemming materials having macroscopic air voids.

- It is not necessary to consider boundary layer growth effects in flow into an initially-evacuated LOS; the approximation of instant mixing of ablation products is adequate.

- Slifer cables, even those of the "low-threshold" type, appear to indicate shock arrival significantly later than it actually occurs at sub-kilobar LOS vapor pressures.

- A front end employing tuballoy in order to produce slower LOS flow may be necessary in the proposed Dirtball event if fast closures are expected to protect samples from plasma.

SECTION 5
LOS ENERGY FLOW SIMULATION

Moore and associates at Physics International (Reference 10) have carried out a series of high-explosive simulation experiments designed to gain understanding of how asymmetries may be employed to minimize energy flow in the line of sight. This could lead to more effective and economical sample protection hardware, especially for low-yield testing. Members of the S^3 scientific staff participated in the selection of experimental configurations and in post-test analyses. This included carrying out calculations of the performance of some of the configurations tested. This section discusses the current level of understanding, the calculations performed to date, and recommendations for future experiments.

5.1 SUMMARY OF EXPERIMENTAL RESULTS

The experiments performed by PI investigated the effect of various asymmetries on target damage. The asymmetries were superimposed on standard thin steel pipes which were evacuated in all but several cases. Spiral asymmetries of various types were used, as either an external wrap around the pipe or an internal liner. Several complete cylindrical liners or wrappings were also tested.

The experiments were of two types. The first, called the APC series, employed pipes which were collapsed by the detonation of a cylindrical charge of nitromethane surrounding a significant length of the pipe, (Figure 5.1). The detonation was initiated at one end of the pipe and it drove a propagating collapse which in some cases led to the jetting of energetic material. The damage caused to a witness plate at the other end of the pipe was one qualitative measure of the jetting. Other diagnostics were employed as well. In particular, flash x-ray pictures were unable to identify the jet, particle spray, or other agent that damaged the target plate. The other type, called the LS series (Figure 5.2), employed a spherical charge of nitromethane

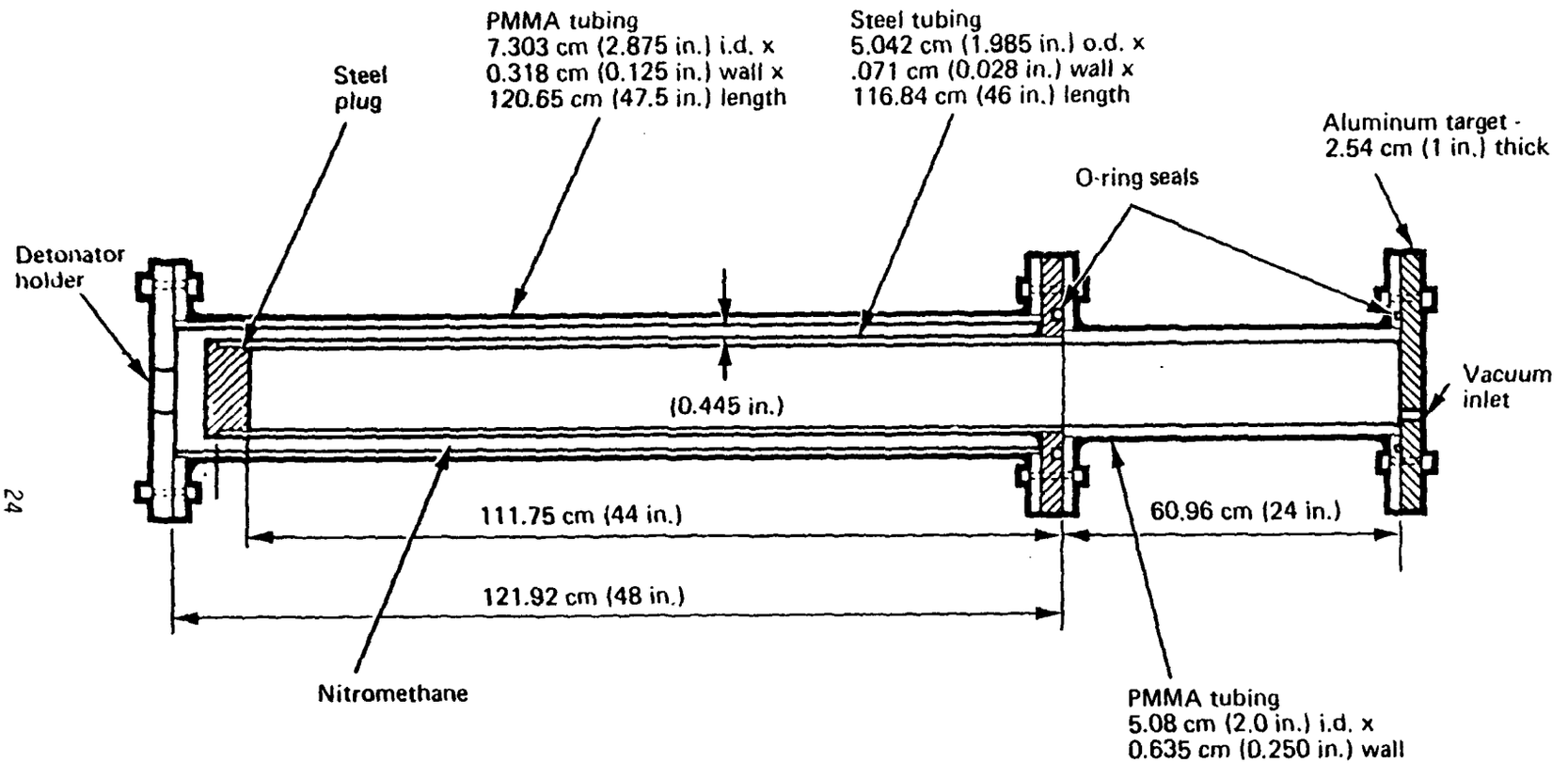

Figure 5.1 Configuration of the APC-1,2 Explosive Driver Experiments. [Longer transparent PMMA extension tubes were used for APC-3 through 10. The figure is taken from Reference 10]

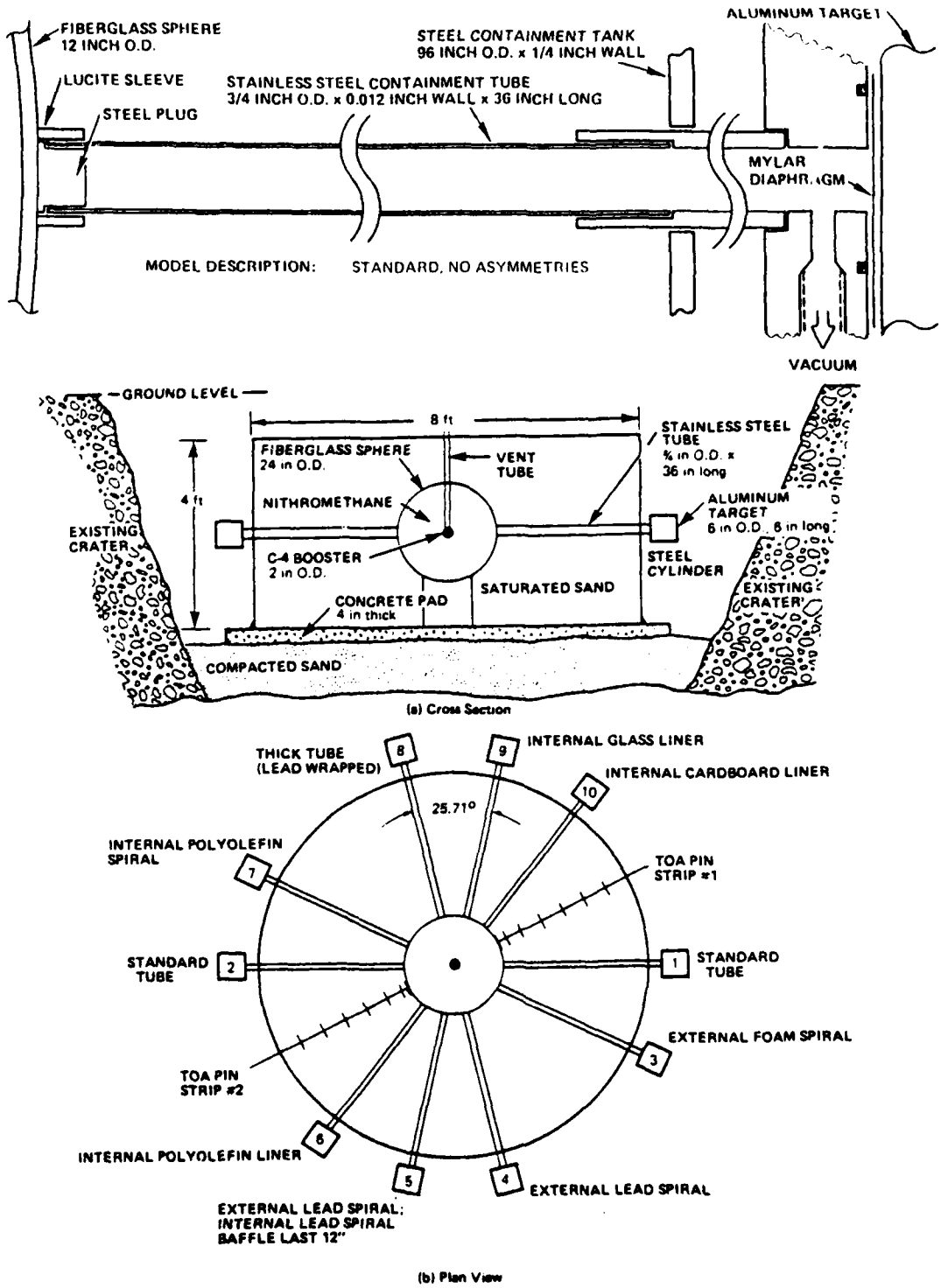

Figure 5.2 Configuration of the LS-II Experiment. Standard Model Shown; Other Models are Variants of This. [This Figure is taken from Reference 10]

embedded in a large container of saturated sand. This drove a spherically divergent shock in the sand, similar to the situation in an underground nuclear test. A number of pipe configurations, extending in various directions from the sphere, were employed on each test. Witness plates at the end of each were again useful in assessing the jetting.

Reference 10 describes in great detail the configurations tested in the APC series and in the LS-I and LS-II experiments. LS-III has since been carried out, adding greatly to the data base (Reference 11). Only a brief summary of the results will be given here. Table 5.1 summarizes the APC series and Table 5.2 the LS series. The conclusions can be simply stated:

APC Series

- An external spiral asymmetry drastically reduces damage to the target in evacuated pipes.

- The presence of 1 atm air in the standard cylindrical pipe drastically reduces damage to the target.

LS Series

- An external spiral asymmetry or an internal axial strip asymmetry produces no qualitative reduction in damage to the target.

- An internal spiral asymmetry drastically reduces damage to the target.

- A heavy symmetric lead wrap produces increased target damage.

- In the only configuration employing 1 atm air in the symmetric pipe, target damage was substantially increased. This configuration was also unique in employing a substantially thicker steel pipe.

Table 5.1. Summary of Physics International Co.'s APC Experiment Series*

Experiment Number	Special Feature	PMMA Extension Tube o.d.(cm)	PMMA Extension Tube length(cm)	Target Damage
APC-1	Standard, short extension tube	6.35	60.96	Total penetration of 2.54 cm target with 5.08 cm dia. hole
APC-2	Same as 1	6.35	60.96	Same as 1
APC-3	Standard	5.72	121.92	Total penetration of 10 cm target
APC-4	Standard, more diagnostics	5.72	121.92	Same as 3
APC-5	Lead spiral wrap on driver tube	5.72	121.92	No target damage
APC-6	1 atm air in tube	5.72	121.92	No target damage
APC-7	Foam spiral wrap	5.72	121.92	Slight target damage
APC-8	Square pressure tube and extension tube	6.35 (square)	121.92	Modest target damage
APC-9	Stainless steel driver	5.72	121.92	Same result as Standard
APC-10	Scalability test - driver dimensions 3/8 of Standard radially unchanged axially	3.81	121.92	No damage. Suspect jet expanded in large diameter extension tube
APC-11	Full scaling test - all dimensions approx. 3/8 of Standard	2.22	46.05	1.905 cm hole to depth of 8.4 cm; hole volume = 29.6 cc

*Configuration was as in Figure 5.1 with ambient pressure 1 to 2 mm Hg except as noted. This material is condensed version of Table 1, Reference 10.

Table 5.2. Summary of Physics International Co.'s LOS Simulation Experiment Series

[LS-1 results, discussed in Reference 10, were clouded by loss of sand penetration and unplanned asymmetries and are not regarded as definitive.]

LS-II

Model	Variations on Standard (Dimensions in cm)	Target Damage		
		Penetration Depth, cm	Hole Volume, cc	Hole Diameter, cm
1	Standard	5.8	16.5	2.2 to 2.4
2	Standard	3.4	9.1	1.5 to 1.6
3	Low density foam external spiral wrap, 3.65 pitch x 0.99 wide x 0.24 thick	4.2	13.6	2.2 to 2.9
4	Lead external spiral wrap, 3.65 pitch x 0.89 wide x 0.20 thick	4.2	17.0	2.0 to 2.6
5	Same as 4 plus internal lead spiral baffle 5.08 pitch x 0.32 wide x 0.32 thick, last 30.5 cm of pipe	0 (some small pits)	0	0
6	Cylindrical polyolefin liner (1 g/cc) 0.036 thick	7.2	17.2	1.9 to 2.0
7	Polyolefin internal spiral 5.08 pitch x 1.27 wide x 0.036 thick full length of pipe	0 (some small pits)	0	0
8	External cylindrical lead wrap 0.20 thick, full length	9.2 (hole completely through target, volume is lower limit)	37.2	2.3 to 2.5
9	Cylindrical glass liner 0.051 thick	7.7	31.5	2.3 to 2.7
10	Cylindrical cardboard liner 0.046 thick	5.8	10.6	2.1 to 2.4

SUMMARY OF RESULTS, LS-3

PURPOSE OR PARAMETER	MODEL POSITION	MODEL TYPE (3/4-in. o.d. 321 stainless steel tubes)	TARGET DAMAGE	
			PENETRATION, cm	HOLE VOLUME, cm^3
		LOS MODELS (0.012-in. wall, internal pressure < 0.75 mm)		
Reproducibility of Standard	1	Standard No. 1	4.4	13.0
	10	Standard No. 2	6.2	25.0
	11	Standard No. 3	6.3	33.0
	14	Standard No. 4 (without pins)	4.8	22.0
		Average	5.4	23.3
Reproducibility of Polyolefin Spiral	7	Poly Spiral No. 1	-- Pitted Surface	--
	8	Poly Spiral No. 2	-- Pitted Surface	--
	17	Poly Spiral No. 3	-- Pitted Surface	--
Effect of Materials	6	Steel Spiral	-- Pitted Surface	--
	5	Lead Spiral	-- Relatively Smooth	--
Effect of Geometry	13	Straight Polyolefin Strip	6.3	11.4
Effect of Baffle	12	Thick Lead Spiral Last 15 in. (baffle)	-- Less pitted than poly or steel	--
Source Resolution	2	Standard with 4-in. Standoff	5.3	15.5
	3	Standard with 8-in. Standoff	4.0	11.5
	4	Standard with 12-in. Standoff	2.7	8.4
	15	Polyolefin Spiral – first 6-in. only	3.9	12.2
	16	Polyolefin Spiral – first 9-in. only	1.2	2.8
		PINEX MODELS (0.028-in. wall, internal pressure 760 mm)		
Simulate Pinex Pipe	20	Standard	14.9	61.5
	19	Polyolefin Spiral	-- Pitted Surface	--

Table 5.2 (Continued)
[This table was provided by E.T. Moore, Reference 11]

- The standard symmetric configuration was used six times to check repeatability; a wide scatter was observed in the results.

We have analyzed the "Standard" LS results statistically. These include LS-II-1,2 and LS-III-1,10,11,14. The average hole volume for these six was 19.8 cc. Three other experiments using thin symmetric liners inside the Standard pipe (II-6, polyolefin; II-9, glass; and II-10, cardboard) also gave an average hole volume of 19.8 cc. It could be argued that these are properly part of the Standard set. The standard deviation in hole volume is 8.2 cc (using all nine tests - 7.9 cc using only the six). If a Gaussian distribution is assumed, the curve shown in Figure 5.3 is obtained. The hole volume for the single symmetric Lead Wrap case (II-8) was 37.2 cc, a value which would occur in less than 2 percent of Standard cases if the above distribution is realistic. It can be said that, with high probability, the Lead Wrap configuration causes greater damage to the witness plate than does the Standard configuration.

5.2 CALCULATIONAL STUDIES OF SYMMETRIC CONFIGURATIONS

Before discussing our current understanding of the damage mechanism inferred from these data, it is worthwhile to present the results of the calculational studies. 2-D STREAK calculations were carried out in axisymmetric geometry to study pipe collapse and energy flow in symmetric configurations. There are some notable differences between the calculations and the observations (as well as some notable areas of similarity), and the attempt to understand these has played a major role in the development of our tentative scenario.

Symmetric configuratons which have been calculated include the APC Standard, LS Standard, LS Lead Wrap, LS 12" Standoff, and LS Pinex.

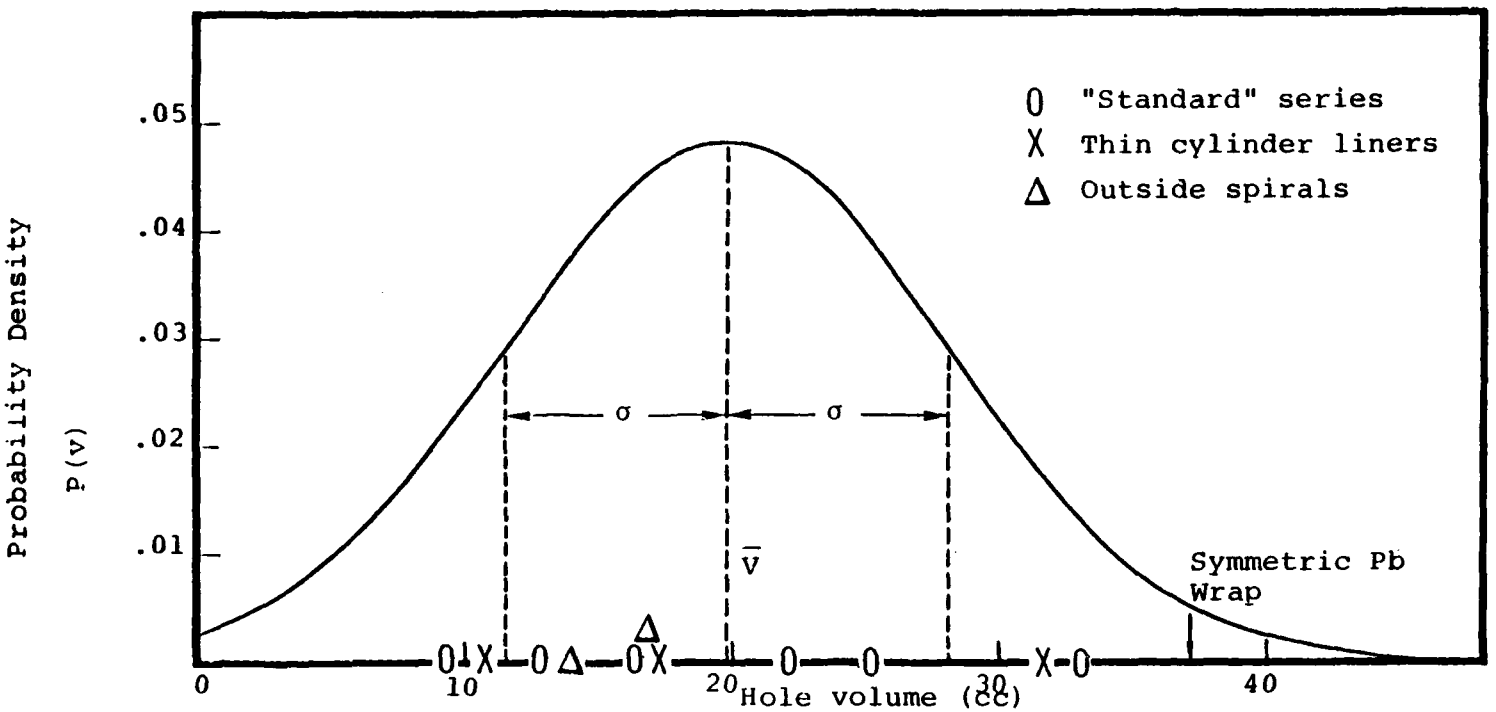

Figure 5.3 Postulated Standard Distribution of Hole Volumes for Standard LS Cases. [$\bar{V}$ = 19.8 cc, σ = 8.2 cc]

APC Standard

Asymmetric calculations of collapse and jetting with this configuration were carried out previously (Reference 12). These were performed in the moving frame of reference of the detonation wave, using the 2-D STREAK code. The steel liner was included. A jet of iron vapor was produced with the properties shown in Figure 5.4. These conditions prevailed in a "throat" region where the portion of the liner that became vaporized by collapse heating near the axis was transferred from the Eulerian material package defining the liner to the package defining the pipe vapor (see discussion in Reference 12). No jet of condensed material was formed in the calculation. These conditions were used as the basis for a FLIP calculation. This was carried out in two stages. In the first stage (HE burn), FLIP was run in the detonation wave frame of reference (6.1 km/sec) with vapor fed in at the throat at 5.6 km/sec with the properties given in Figure 5.4. At the completion of HE burn the FLIP solution was transformed back to the laboratory frame of reference and the calculation was continued until the pressure pulse in the stagnation region in front of the aluminum target (assumed rigid) was completed as shown in Figure 5.5.

It is seen that the calculated arrival was somewhat early. Perhaps this was due to the omission of ablation in the calculation. The calculation was then repeated using the vaporization/scour model of ablation as was standard in FLIP prior to the improvements described in Section 4 of this report. The calculated arrival at the target was somewhat later than observed (Figure 5.5), suggesting that the ablation produced by the model then in use was excessive. This is consistent with the findings of Section 4. Note that the two calculated impulses were not very different.

It was concluded that a pressure pulse far above the yield point of the aluminum target was produced. However, a satisfactory mechanism whereby this pulse could punch a hole in the target of the same diameter as the pipe has not been devised. Our present feeling is that

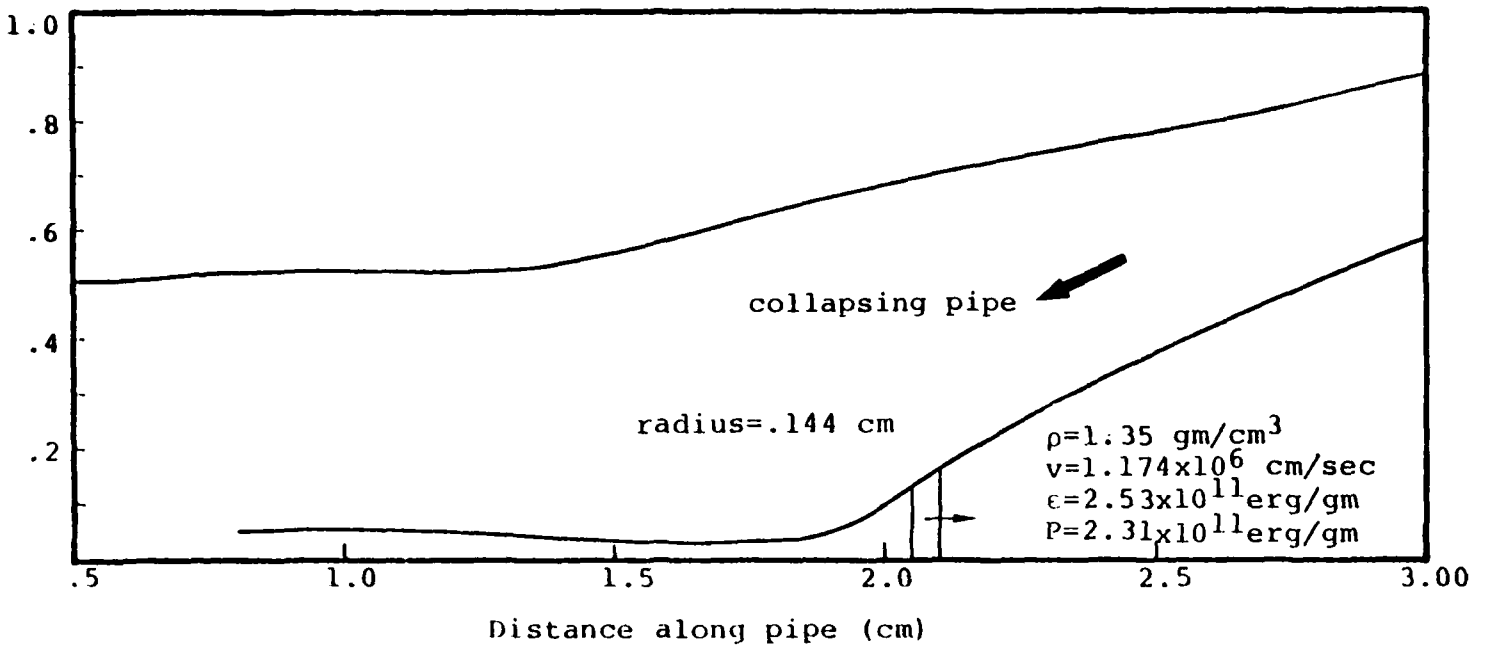

Figure 5.4 Configuration of imploded pipe driven by nitromethane at 1.65 μsec in a calculation using the vaporization-condensation model. ρ, v, ε, and P are properties of "jet" in band between 2.05 and 2.10 cm. This calculation was done in a moving coordinate system.

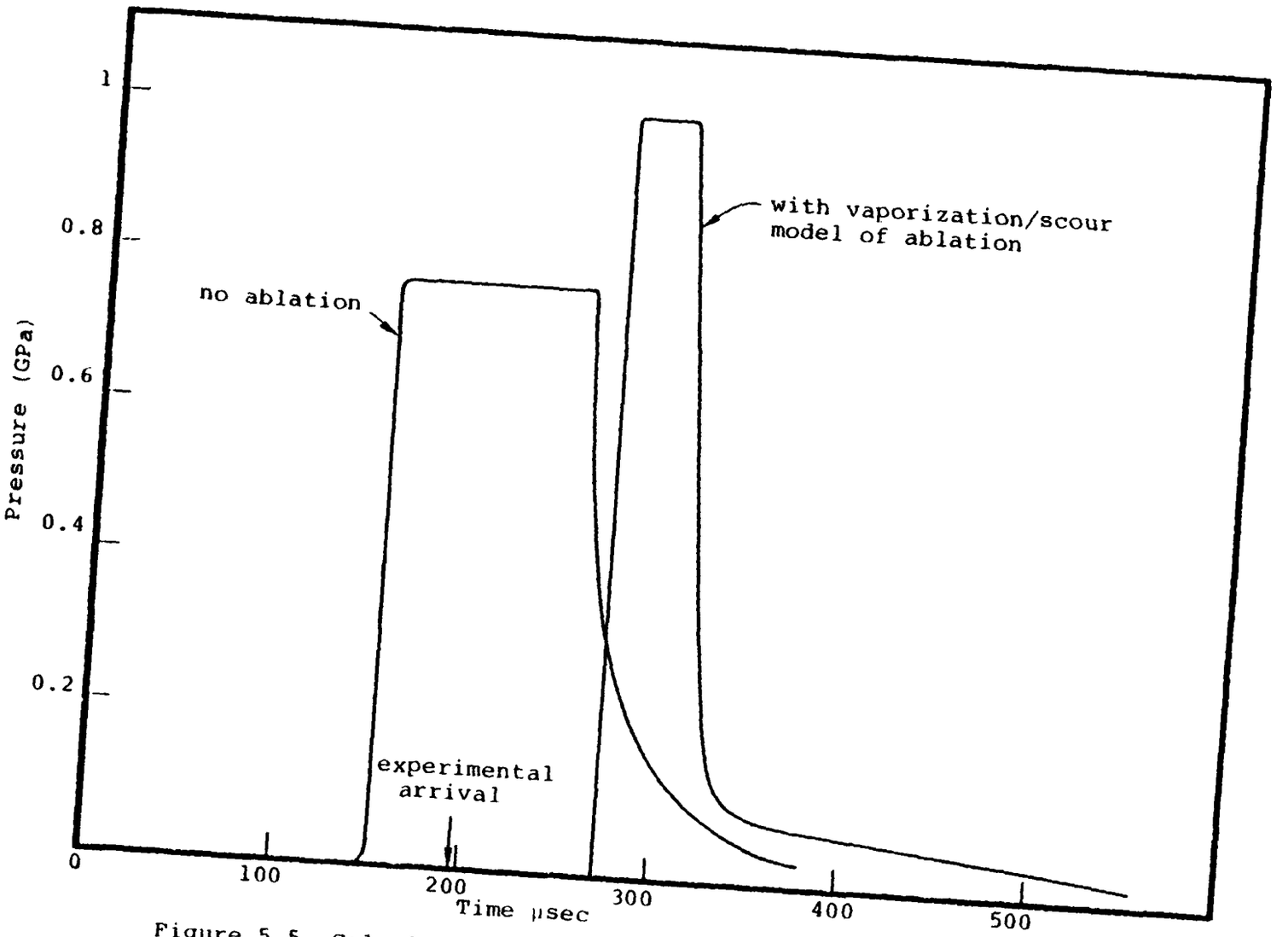

Figure 5.5 Calculated Pressure at Aluminum Target Plate, APC - 1,2

pipe rupture at the target would vent the pressure and that the hole was made by a jet of particulate matter. Such a jet has not been seen in x-ray diagnosis, implying that the maximum particle or droplet size is 25 μm (Reference 10). Such a jet is not indicated in the calculation, probably because much finer zones would be required to permit it to initiate. (See discussion in Section 5.3.)

LS Standard

In the calculations of the LS configurations performed so far, the steel liner has not been included*. These 2-D STREAK calculations include the late-time motion of the HE products and a description of the "ground" shock in the wet sand which drives the pipe collapse. Hence, only ten radial zones to describe the pipe radius were practical, compared with twenty in the APC calculations. However, the ground shock pulse driving LS collapse is much longer lasting than the direct HE pulse driving APC collapse, and it was determined that the small liner mass would not have a significant effect on the collapse rate. Vaporization of that liner was included in the calculation and was the source of the energetic vapor flow as in the APC calculation. The fact that the source of the vapor in the LS calculation, strictly speaking, was the wet sand, seems unimportant because the specific internal energy in the axial collapse region depends only on the collapse velocity to a good approximation. The vaporization enthalpy appropriate for iron must, of course, be used in determining the amount of liner vaporization.

*The method used in the APC calculation which permitted the pipe wall to be included conveniently could not be used for the LS series because there is no frame of reference in which the collapse is steady in a spherically divergent geometry.

The LS series of calculations was performed after the improved ablation model discussed in Section 4 had been developed and had been added to STREAK to give it the capability formerly possessed only by the quasi-1-D FLIP code. Initialization was at 50 μsec, the completion of HE burn, with the solution of a 1-D spherical HE burn calculation overlaid on STREAK. The "Standard" calculation was carried to 290 μsec. It produced an iron vapor flow qualitatively similar to that determined in the APC case. The time evolution of the energy in this vapor flow is shown in Figure 5.6. The calculated time of arrival of the vapor flow at the witness plate, 180 to 190 μs compares well with the measured time of 170 to 180 μs (Reference 10). A jet of wet sand emanating from the collapse point was also produced - see the plot of tracer particles defining material boundaries, Figure 5.7 The time history of the energy in this jet is also shown in Figure 5.6.

The sand jet appearing in calculations such as this has been regarded in the past as qualitatively representing reality. In particular, for LOS calculations, the pipe typically expands to several times its initial diameter ahead of the collapse point as a result of internal vapor pressure. This would surely rupture the pipe in many places, exposing the surrounding stemming material. The eventual collapse should lead to jetting of the stemming. On these HE simulations, things are not so clear. The maximum pipe expansion seen ahead of collapse is about 0.3 initial diameters, only marginally enough to rupture the pipe. (Although pipe strength is not included in the calculations, it is insufficient to alter this finding.) The collapse process may cause jetting of only the pipe wall (liner) material. The liner may effectively block jetting of the stemming sand. It was hoped that, in such cases, the calculated sand jetting energy would be comparable to the actual liner jetting energy and that comparisons of calculations of different configurations using the same zoning would provide reasonable comparative estimates of the energies in their jets. As the later discussion indicates, that this hope was probably not fulfilled.

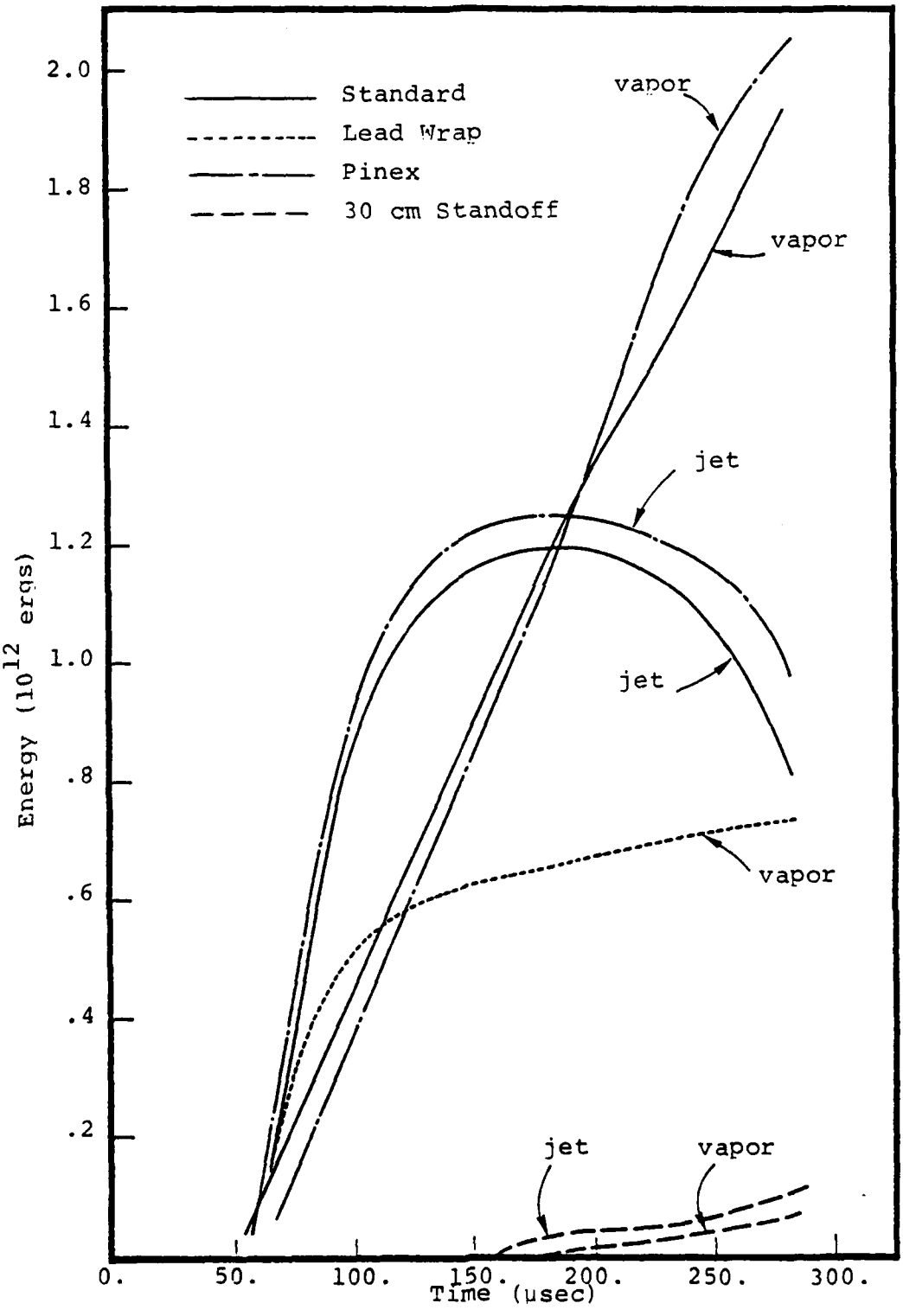

Figure 5.6 Energy Evolution in Vapor and Condensate Jet for LS Calculations

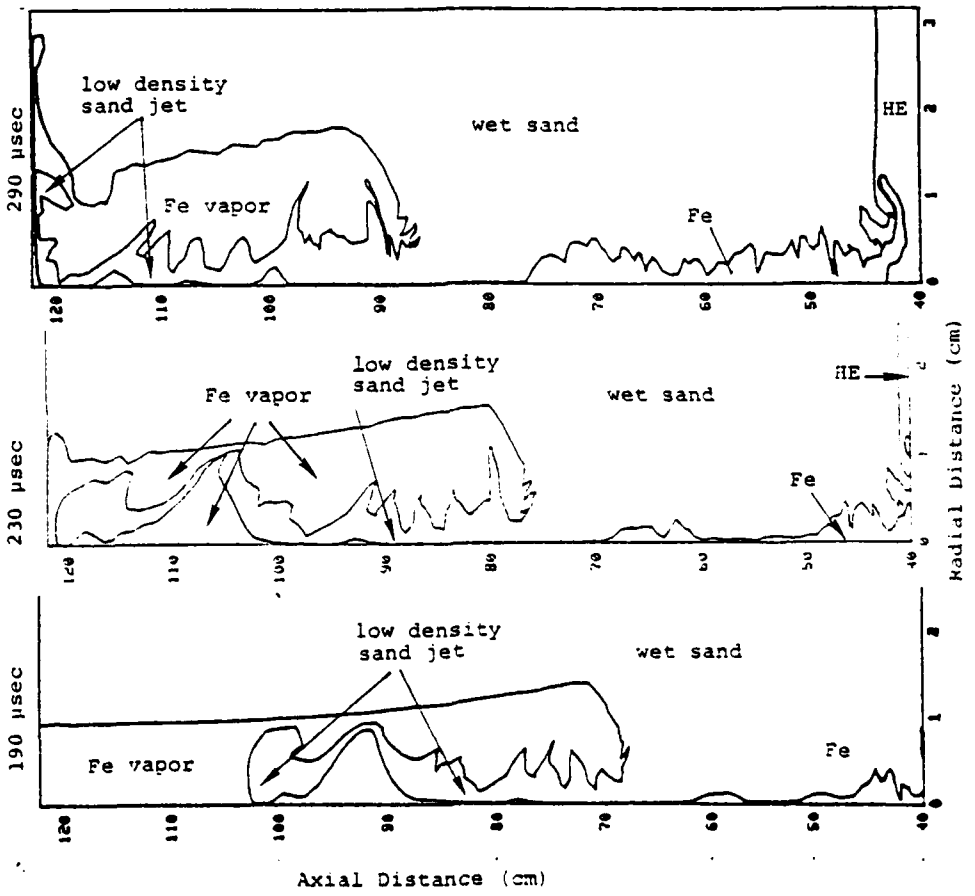

Figure 5.7 Evolution of Material Boundaries in the PI "Standard LS" Case

The literature on hypervelocity impact cratering was consulted to determine whether the measured hole volumes in LS witness plates could be understood in terms of the energy in the jet. The major difficulty in applying those results is that the cratering data apply to single projectiles of the order of 1 mm diameter and larger, whereas the sand jet is envisioned as a shower of particles, mostly much smaller than 1 mm. Nevertheless, it was learned (References 13-15) that, for impact velocities in the range of about 4 to 6 km/sec - which STREAK gives for the sand jet - the ratio of impact kinetic energy to hole volume in an aluminum target is reasonably constant at about 7×10^9 ergs/cc. This is for aluminum projectiles. In the present case the projectiles would be silica; their density, which is the dominant parameter in cratering considerations, is close to that of aluminum. The average hole volume of about 20 cc in the Standard case would imply an incident kinetic energy of 1.4×10^{11} ergs, which is comparable in order of magnitude with the calculated results. (About half the jet energy shown in Figure 5.6 is kinetic.) There is no possibility of a realistic quantitative comparison because, with a shower of projectiles, there is interaction between the shock waves which they generate in the cratering process.

In summary, the calculated energy in the sand jet appears capable of explaining the target damage. Other explanations may be more plausible when considered in the context of all of the calculations plus the data - see Section 5.3.

Lead Wrap (LS-II-8)

A calculation of the symmetric Lead Wrap case was carried out on STREAK using the same zoning as in the Standard case. This calculation was carried to 371 μsec. No jet of condensed material is seen in this calculation - see the plot of material boundaries, Figure 5.8. The slower moving lead does not get ahead of the collapse point.

In the experiments, the hole in the witness plate in the Lead Wrap case was significantly deeper than in the average of the Standard

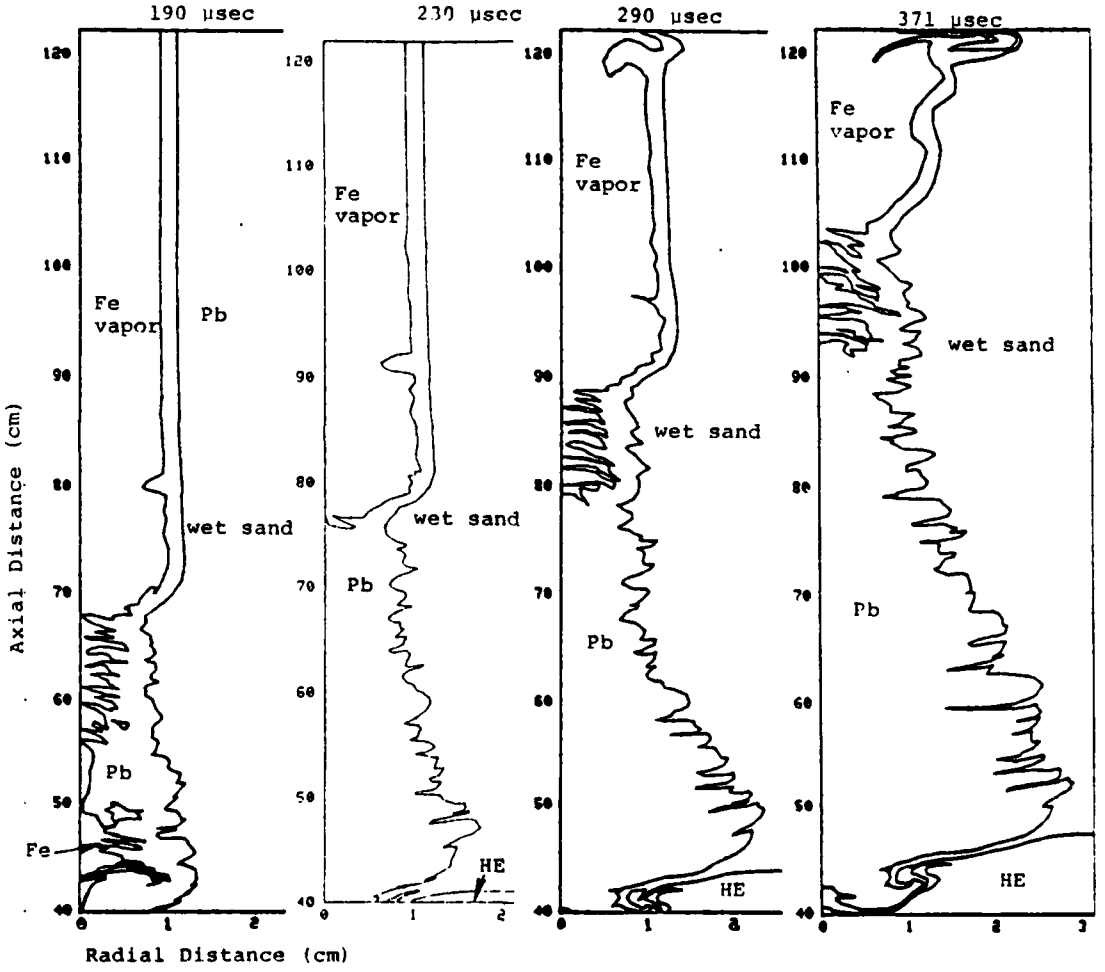

Figure 5.8 Evolution of Material Boundaries in the Calculation of the "Lead Wrap" Case

cases. The obvious features ahead of the pipe collapse point in the calculations would lead us, in the absence of experimentation, to expect the opposite. Even the calculated energy in LOS vapor flow is substantially lower than in the Standard case - see Figure 5.6. The damage in the Lead Wrap case could be due to the moving slug of lead in the collapsed region (Figure 5.8). The calculational edits strongly suggest that the central core of this is in a molten state, about 500 grams carrying 2.7×10^{12} ergs of which 2×10^{11} ergs is kinetic energy. The pipe collapse region in the Lead Wrap case appears nowhere near as competent as that in the Standard case, where the collapsed region (except fairly near the source) is clearly indicated by the calculations to be in a solid, recompacted state. Nothing stands between the witness plate and the molten lead.

However, the average velocity in the molten lead slug is only 0.2 to 0.3 km/sec. Although it is energetic enough to do substantial damage to the witness plate, the estimated velocity of the witness plate after reflection of the ground shock is comparable to that of the lead slug and the plate would be significantly displaced, and the pipe-witness plate junction long severed, before arrival of the lead slug. The iron vapor pressure may cause this kind of disruption even earlier. Note the expansion already present near the end of the pipe in Figure 5.8. (The calculation, of course, cannot represent rupture.) It seems unlikely that the observed hole in the witness plate, which matches the pipe diameter, could be made by the lead slug.

In summary, the calculation does not provide a plausible mechanism for the observed damage to the witness plate in the Lead Wrap case.

30.5 cm Standoff (LS-III-4)

In this case the steel plug (see Figure 5.2) was located 30.5 cm from the HE charge. The lucite tube between the plug and the HE had many holes drilled in it and was filled with wet sand. This region was regarded as all wet sand in the calculation, which was carried to 357 μsec.

The Standoff case, as expected, has the same qualitative features as the Standard case but with less energy. Since the peak stresses experienced at the pipe are much lower than in the Standard case, much less iron vapor is generated by the pipe collapse. Its energy content is about two orders of magnitude below the Standard case (Figure 5.6). A jet of sand is generated by the collapse process (Figure 5.9) with energy about a factor of ten below the Standard case (Figure 5.6). It is noteworthy that the peak free-field stress level in the wet sand is about 18 kbar (1.8 GPa) at the beginning of the standoff pipe, versus about 175 kbar (17.5 GPa) at the beginning of the standard pipe.

The observed ratio of hole volumes in the Standard and 30.5 cm Standoff cases is about 2.5 to 1. This is considerably lower than the calculated ratio of sand jet energies. However, the average jetting velocity is somewhat lower in the Standoff case, and it is known that the ratio of crater volume to impacting energy increases at lower velocities (References 13-15) because the crater ejecta are less energetic. Furthermore, there may be considerable variation in the hole volume if a number of duplicate Standoff configurations were tested, as was the situation with the Standard configuration. Therefore, the calculational comparison of the Standard and 30.5 cm Standoff cases may not be inconsistent with the experimental results.

Pinex (LS-III-20)

The Pinex configuration was identical to the Standard except that the pipe contained air at 1 atm, whereas the Standard was evacuated, and the Pinex pipe was steel, 0.71 mm thick, whereas the Standard pipe was steel, 0.30 mm thick.

The Pinex calculation did not model the pipe mass; the only difference from the Standard calculation was the ambient air. The Pinex calculation produced only slightly more energetic vapor and sand jetting than the Standard. Figure 5.6 shows the calculated vapor and jet energies. The calculated jet energy increase can be attributed to the

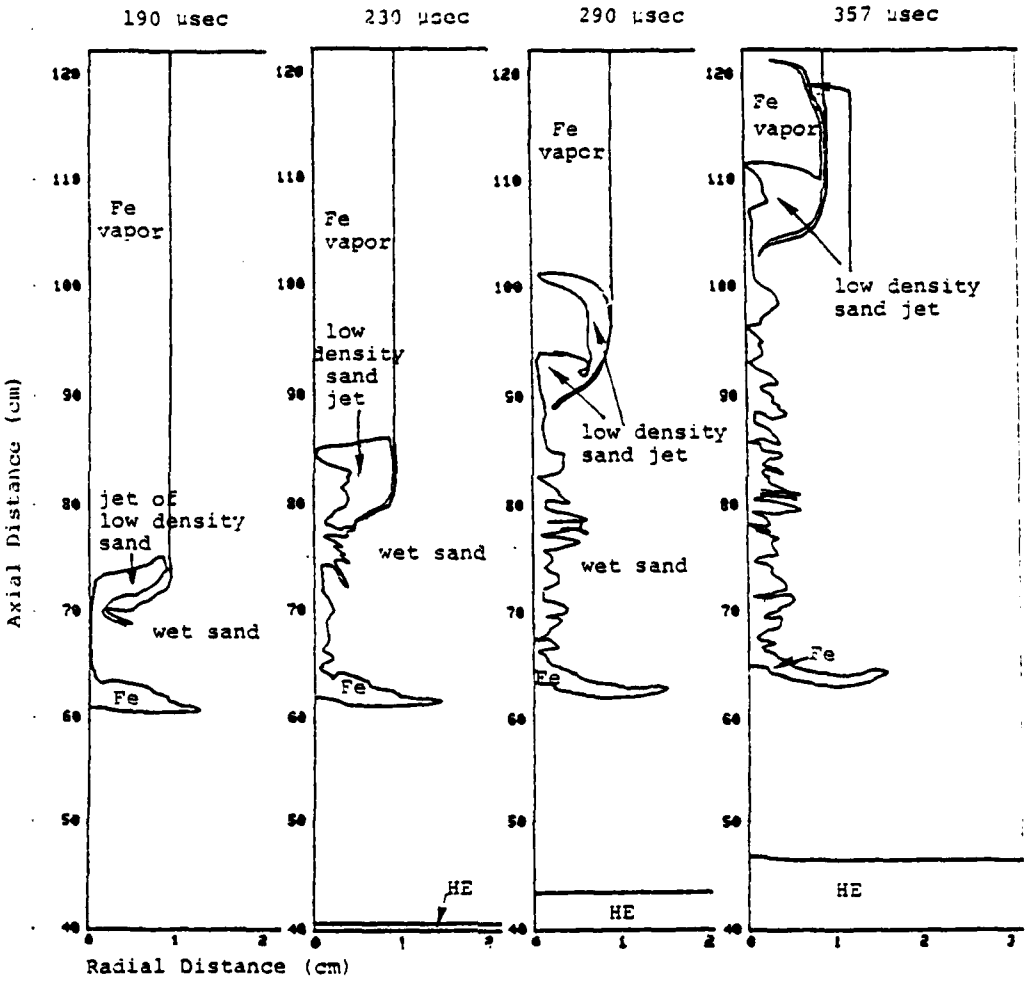

Figure 5.9 Evolution of Material Boundaries in the Calculation of the PI "12 inch Standoff" Case

fact that a shock propagates in the ambient air, and the vapor region driven ahead of the collapse is at higher pressure than in the Standard case, hence more work is done on it. Greater pipe expansion occurs and the jetting accompanying collapse is more energetic. The observed hole volume in the Pinex case, however, was over three times the average of the Standard cases. The calculational results do not suggest more than a modest increase in target damage. This contradiction suggests that the difference in the steel liner thicknesses is responsible for the observed differences in the target damage.

5.3 A SCENARIO FOR THE PERFORMANCE OF THE SYMMETRIC CONFIGURATONS

The initial hope of obtaining a good understanding of the symmetric PI experiments with the help of reasonably economical calculations has not been fulfilled. Comparison of the calculations with the data suggests one of two possibilities. Either the calculations do not model some physical process correctly, or they omit an important feature of some configurations. We will show that the evidence suggests the latter, namely the omission of the liner (steel pipe plus other materials) which could produce jetting of condensed material. This material, either in the form of liquid droplets or loose solid particulates, could produce the observed hole volumes by hypervelocity impact.

Some vaporization of the liner material can occur on collapse. This already appears to be adequately represented in the calculations, as discussed above. This is not thought to be the principal mechanism of target damage because its variation among the configurations does not correlate well with the damage variation.

The jetting of condensates is well understood, at least qualitatively. The theory of jets produced by collapsing plates, (Reference 16) which is also successfully applied to collapsing conical liners, gives the jet velocity, V_j, and the jetting mass per unit axial length of liner, m_j. The resulting formulas are particularly simple for the cylindrical liner case:

$$V_j = 2V_d$$

$$m_j = m \sin^2 \beta/2$$

where V_d is the velocity of the driving detonation or shock (which propagates in the axial direction), m is the liner mass per unit length, and β is the collapse angle - see Figure 5.10. For thin liners driven by a shock in an infinite medium, β is expected to be a function only of the surrounding medium and the driving wave strength. Therefore, β should be about the same at any given range from the HE source for all the symmetric LS configurations except possibly the Lead Wrap. For a given variation of V_d with range the above model suggests a postulate that the energy in the jet, and therefore the hole volume, is directly proportional to m. This postulate is reasonably consistent with the comparison of liner mass and target damage (hole volume) for the symmetric LS configurations given in Table 5.3. The Lead Wrap case is the only one that is clearly inconsistent with the postulate. The comparison between the Standard and Pinex (LS III-20) cases is especially noteworthy. The postulate is also consistent with the Standoff experimental results (LS-III-2,3,4) because the shock and implosion are weaker at greater distance, implying a lower jet energy (lower V_j).

The Lead Wrap case more nearly fits the above correlation if the β term is properly adjusted. The other calculated cases all show approximately equal β's at any given range, with values varying from about 11° to 17°. In the Lead Wrap case β varies from about 8° to 12° because of the slower collapse velocity. The ratio of the $\sin^2 \beta/2$ terms suggest that m_j should be reduced about a factor of two to three for the Lead Wrap, which would imply that the hole volume should be 4 to 6 times the Standard. However, it would be unreasonable to discard the liner hypothesis on account of this. First, the Standard results produced a wide variation of hole volume, the largest being more than three times the smallest. We have only one result for the Pb wrap. Second, simple theory assumes impulsive loading of the liner,

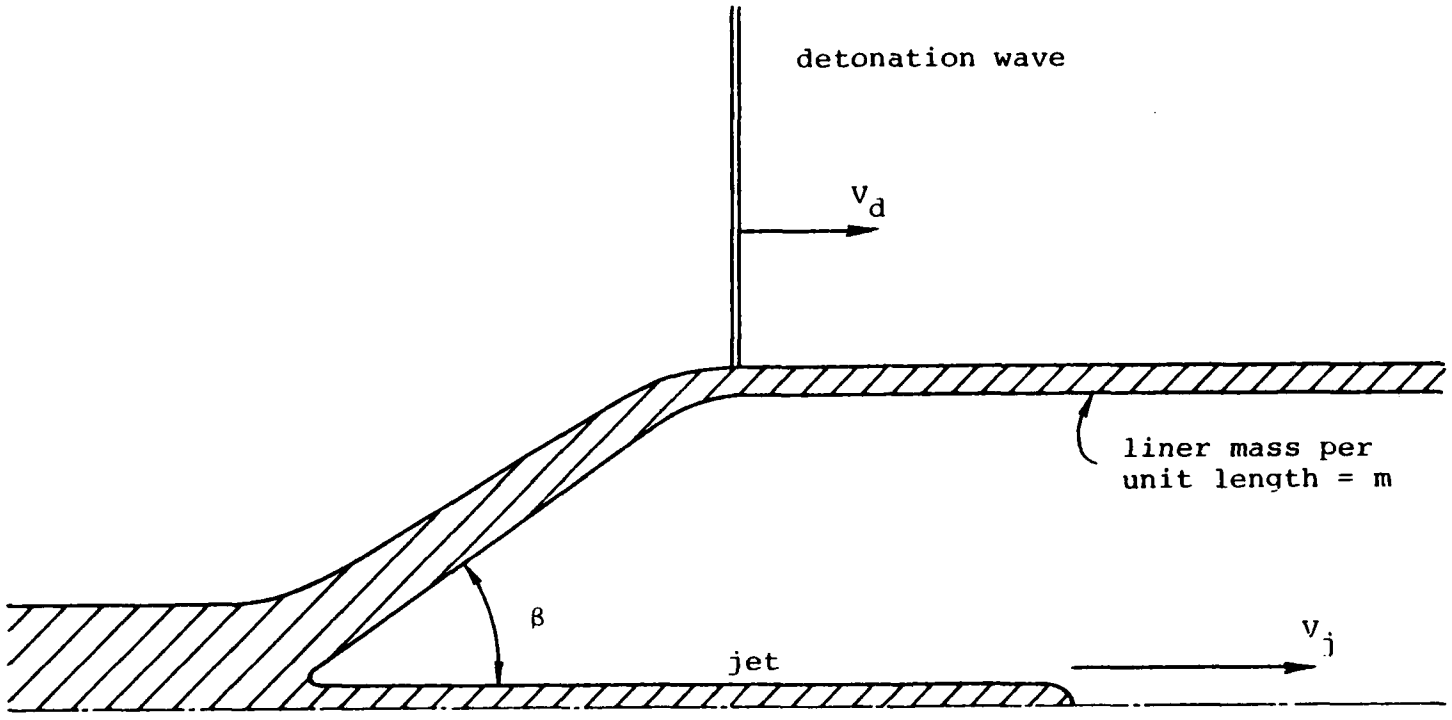

Figure 5.10 Symmetric Liner Jetting Geometry

Table 5.3 Liner Mass per Unit Length for Symmetric LS Configurations and Comparison with Hole Volumes in Witness Plates

Case	Liner Description*	Liner Mass g/cm	Liner Mass / Standard	Hole Volume / Standard Average
LS-II-8 (Lead Wrap)	Pb 2.032 mm steel 0.305 mm	16.7	11.8	1.88
LS-III-20 (1 atm air)	steel 0.711 mm	3.30	2.33	3.11
LS-II-9 (glass liner)	steel 0.305 mm glass 0.508 mm	2.07†	1.47	1.59
LS-II-6 (polyolefin liner)	steel 0.305 mm polyolefin 0.356 mm	1.62†	1.14	0.87
LS-II-10 (cardboard liner)	steel 0.305 mm cardboard 0.457 mm	1.57†	1.11	0.54
LS Standard	steel 0.305 mm	1.41	1	1

*outer material shown first

†estimates - used densities 2.3 glass, 1 for polyolefin, 0.6 for cardboard

not the sustained push from a shock in saturated sand. If the simple theory were taken literally, an infinite Pb medium around the pipe would lead to infinite jetting energy. And third, it is difficult to interpret the calculations in terms of conical collapse since β changes as the process proceeds.

This leads into the question of what should be counted in the "jettable" mass when a liner is surrounded by an extensive medium. If some of the lead wrap should be included, why not some of the surrounding sand in the thin liner cases After all, the Standard case calculations indicate some molten sand near the axis in the collapsed region. This is in contrast to the situation in shaped charge jetting, for which the simple theory above was devised - in that there are only vaporous HE products outside the liner.

Perhaps Rayleigh-Taylor instability also plays a role in the collapse process. When the collapsing motion is stopped by the convergence on axis, the inward motion of the interface between the liner and the surrounding medium is strongly decelerated. This interface is unstable if the surrounding medium is denser than the liner, e.g., lead/steel. For the sand/steel case it should be stable. Also, the lead is quite weak compared to recompacted sand and much more easily melted. In the three cases using thin internal liners with steel pipe outside, instability would be expected at this interface. It could be conjectured that a surrounding material can participate in the jetting only if the interface is unstable. As is usual in such complicated phenomena, it is much easier to state conjectures than it is to prove them. It can only be said that, in general, target damage correlates reasonably well with total liner mass, including some of the thick Pb wrap but never including any surrounding sand.

The presence of 1 atm air produced opposite results in the APC and LS tests. No discussion of the symmetric results is complete without dealing with this question. The above scenario, based on the

aggregate of LS experimental and calculational results, suggests that air has little influence, and the thicker liner in the Pinex case was responsible for the greater target damage. But why did ambient air lead to such a great reduction in damage in the APC-6 case? The only apparent explanation is that the driving pulse is much briefer in the APC series than in the LS series and the imploding momentum is quite modest. (See the more detailed discussion of this in Section 5.4.) The compression of air in the collapse region may be able to prevent the liner from reaching the axis and jetting in the APC case but not in the LS case. (The air-filled APC case has not been calculated.)

The zoning required to calculate condensed phase jetting from a thin liner is quite fine. Consider, for example, the LS Standard case. The steel liner, with the inner radius of 9.22 mm and a thickness of 0.305 mm, would collapse to a radius of 2.37 mm ignoring compression. Taking $\beta = 17^{\circ}$ and again ignoring density changes, the jet radius is 0.35 mm. If the radial zone size is not somewhat smaller than this, the majority of liner mass that is moving into the "slug" behind the collapse point will be in the same zone as the jetting mass, and the averaging of their properties in the same zone will prevent or greatly reduce the jet. Experience with shaped charge jetting calculations at S^3 (Reference 17) indicates that at least five or six zones are required over the radius of the emanating jet if jetting is to be seen in the calculations. This would indicate a minimum zone size no larger than 0.07 mm, or about 1/132 of the inner radius. Such calculations are quite costly and should be undertaken with great caution. One or two will possibly be attempted during the follow-on period.

Any conlcusions drawn from the symmetric experiments are subject to uncertainties raised by the large statistical variation seen in the Standard cases. Repetition of the experiments of interest to determine reproducibility would be very useful.

5.4 CALCULATIONAL STUDIES OF ASYMMETRIC CONFIGURATIONS

One basic conclusion of the LS experimental series was that configurations with asymmetries in the form of an external spiral wrap jetted strongly whereas those with an internal spiral did not jet at all. This result was counter to prior intuition and to the findings of the APC series. In an attempt to gain insight, the collapse of various asymmetric configurations driven by pressure in the surrounding wet sand medium was investigated wih the 2-D planar version of STREAK in the plane perpendicular to the pipe axis.

The configuration studied was a cross-section of the standard pipe. The spiral material extended around one-fourth of the perimeter, to match the pitch and spiral width used by PI. A pressure of 30 kbar (3 GPa) was initiated between the outer grid boundary and a circle of 1.16 cm radius - just outside the thickest external spiral. This pressure is the ground shock level at about 30 cm for the HE. It was maintained at the outer boundary for the entire calculation. The steel pipe mass was included in the calculation. Strength was included for the steel and for the lead if any was present. While the calculated configurations are admittedly only a qualitative representation of the experimental configurations, they appear to preserve the essential features. The calculations should be qualitatively reliable in describing the degree of asymmetry in the collapse process, for this is dominated by elementary laws of motion.

The principal results of the study are outlined in Figure 5.11. For the thick lead "spiral" wrap (LS-II-4) the collapse process essentially leaves the lead behind. This strongly disrupts the overall symmetry of the collapse. The same is seen with a postulated thin lead wrap and thin polyolefin wrap. The internal polyolefin spiral (as in LS-II-7) is seen to occlude the pipe quite effectively in the late stage of collapse.

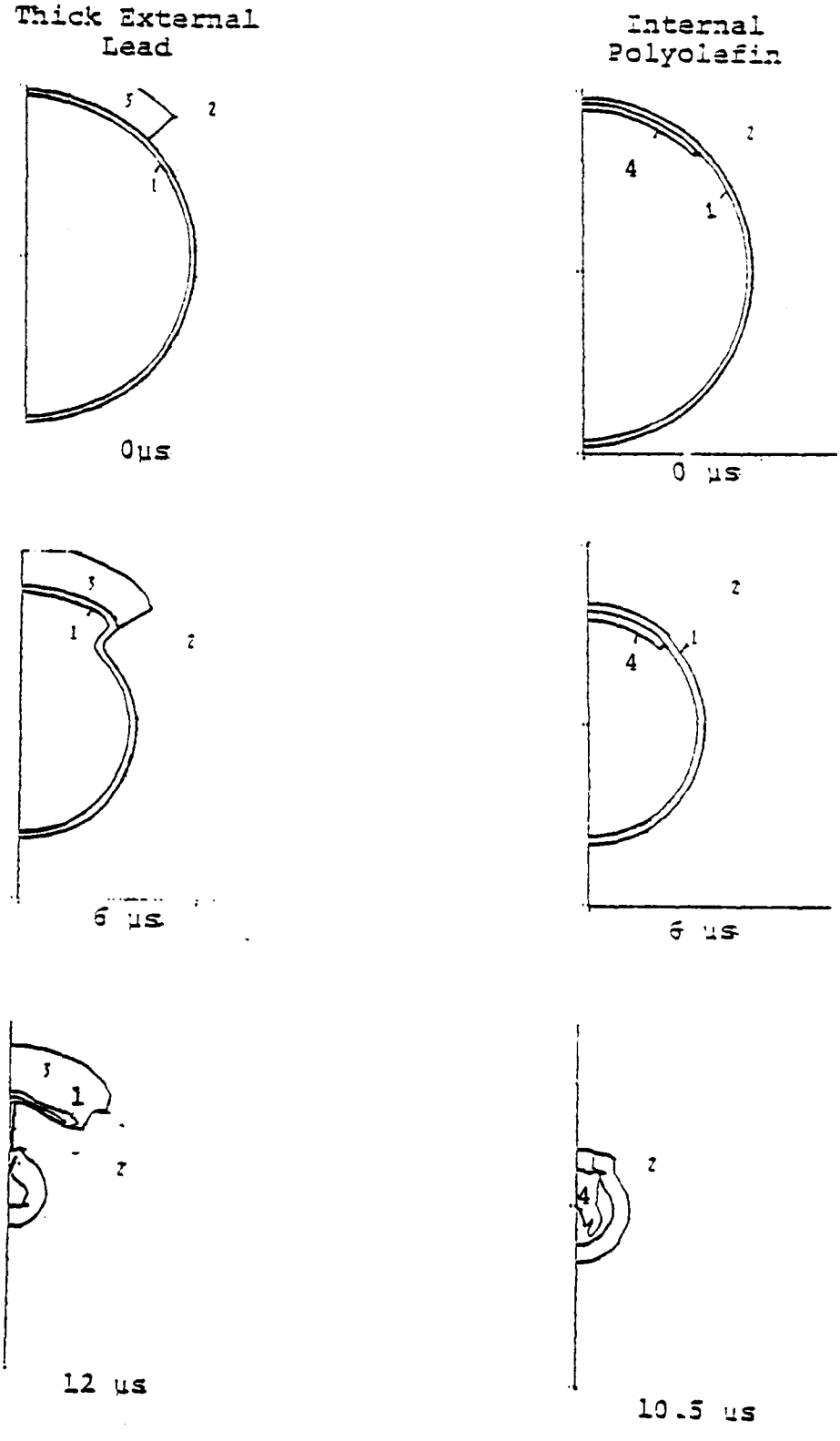

Figure 5.11 Time Sequence from 2-D Planar Calculations of Asymmetric Collapse. Materials: 1 steel, 2 = wet sand, 3 = lead, 4 = polyolefin.

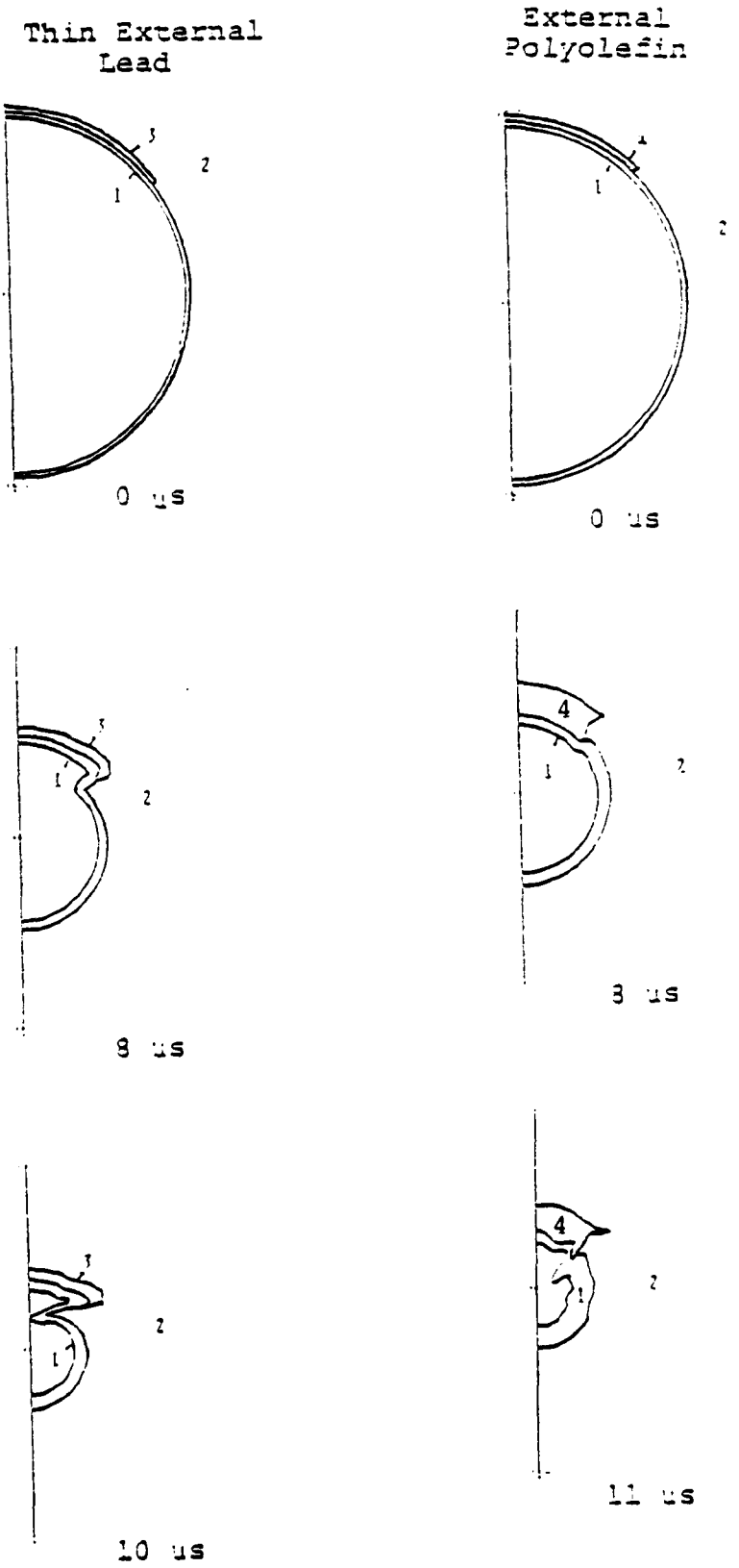

Figure 5.11 (Continued)

At first glance, the collapse in the external wrap cases appears to be quite asymmetric. A closer look, however, reveals considerable local symmetry near the collapse point. The collapse point occurs very near the axis, as the collasping liner material leaves the external wrap behind. The "external polyolefin wrap" calculation, which is similar to experiment LS-II-3, does not show as much local symmetry at the collapse point as the lead-wrap cases. But it is doubtful whether perfect symmetry is required to jet the liner. Even in a symmetric configuration machined to high tolerances, buckling and fluting of the liner are likely to occur on collapse, even if idealized calculations do not manifest them (such calculations have not been performed). This could be the reason for the observed scatter in the Standard LS cases. The local symmetry seen near the collapse point for the external-wrap cases could well be sufficient for liner jetting.

The next question is: Why did the external-wrap APC configurations not jet strongly? It is suggested that the reason for the totally different conclusions about the effects of external wraps in the LS and APC series is related to the differences in the way they were driven. The driving pressure pulse following the shock in the LS wet sand is much longer-lasting than that associated with the direct HE drives in the APC series. Rarefactions need to travel only a short distance through the HE detonation products to relieve the driving pressure on the liner. Evidently, the APC pulse is too short to bring about a high degree of axial convergence. X-rays of the external-wrap APC clearly show asymmetric collapse, well off axis. If the above statements are valid, it would follow that what makes the internal spiral prevent jetting is not the asymmetry of the collapse but either (a) the blockage of the collapse region or (b) the scatter of jetted particles downstream by the spiral. It is not clear that the spiral material does not then become a jet; in postulate (b) it could be the main component of the jet. It is also not clear whether symmetric internal rings would prevent damage to the end plate just as the spiral does. The spiral, unlike the rings, is always present at the collapse

point. An experiment using internal rings would be worthwhile on a future PI test. A finding of minimal target damage would favor postulate (b) above, whereas damage in the nominal range would favor postulate (a).

5.5 IMPLICATIONS FOR UNDERGROUND NUCLEAR TESTS

The findings of these simulation experiments are expected to be applicable at least in the regime of LOS flow which was simulated in the laboratory. In real LOS flow there are at least two phenomena which seem likely to make the results inapplicable at short range from the source. One is the existence of much higher free-field ground shock pressures than the 17.5 GPa (175 kbar) attained near the nitromethane. The other is the possible occurrence of substantial LOS pipe expansion ahead of the advancing closure as a result of high vapor pressure.

For two DNA shots of the recent past, Mighty Epic and Diablo Hawk, the 17 GPa ground shock level occurs at a range of about 13 m. At a range of about 8 to 10 m or less the substantially higher driving pressures lead to calculated maximum pressures of several hundred GPa or more along with high specific internal energies accompanying collapse of the pipe and reverse cone extension onto the axis. This seems sufficient to cause the entire pipe wall and any internal asymmetry to change phase and participate fully in the LOS vapor flow. An alternative view (Reference 18) notes that the viscosity of the shocked material is less than 10^3 poise; if this is so in the LOS case, the asymmetries would be smeared away by the flow. Therefore, spiral asymmetries may not have any effect on phenomena at this range. The evolution of energetic LOS flow, such as outlined in a classified parametric study, may well proceed without hindrance from the asymmetry. The conclusions of that study regarding the superior performance of dense, long extensions are still thought to be valid.

If sufficient expansion of the LOS pipe occurs ahead of the advancing closure, the pipe can rupture, exposing much surrounding stemming. Steel pipe is thought to rupture upon expanding to about 1.3 times its initial radius (Reference 19). Much more expansion than this is routinely seen in 2-D calculations of energetic flow in the LOS. For example, at the end of the calculations for Mighty Epic this had occurred to beyond 30 m and appeared likely to occur to considerably greater range if the calculation had been continued. In this situation any internal asymmetry would probably break in many places and not retain its integrity in the chaotic collapse process. The collapse process would probably result in strong jetting of the stemming material, as seen in the LOS calculations.

According to the calculations discussed in Section 5.2, the greatest expansion attained in the PI Standard configurations was barely enough to cause rupture - and that was probably a slight overestimate since the steel strength was ignored. Therefore, expansion-caused rupture probably did not occur in any significant part of the PI simulation pipes. This raises the question whether the internal spiral would be effective in inhibiting the jetting originating from a region of LOS that is highly expanded prior to collapse. If the internal spiral functions in the PI simulations by blocking the source, it may not be effective in the LOS. If it functions by scattering jetted material downstream from the source, it should be effective in the LOS. Experiments designed to identify the mechanism of the internal spiral operation would be very useful.

Regardless of the true mechanism, an internal spiral asymmetry is likely to perform well if used in conjunction with an optimized design of the near-source LOS. Consider, for example, Diablo Hawk. The pre-shot calculation suggests that pipe rupture ahead of collapse did not occur beyond 20 m, perhaps less, and was not particularly severe at any range. This is because the extension design led to greatly reduced calculated vapor flow. Shrapnel that is thought to be produced by the

jetting of exposed stemming material and/or LOS pipe material, out to a range of perhaps 50 m or more on typical HLOS tests, could potentially be reduced dramatically by the use of an internal spiral asymmetry in conjunction with an optimized close-in LOS design.

CONCLUSIONS AND RECOMMENDATIONS

The following tentative conclusions are based on the experimental data combined with insight gained from calculations:

- The damage to the witness plate on the PI experiments is probably due to the jetting of liner material - the steel pipe plus any symmetric internal liner or external wrap material - in a condensed state. The calculations cannot model this phenomenon without very fine zoning.

- The LS experiments differ fundamentally from the APC experiments in that the pulse driving the pipe collapse is much longer in LS, making mass asymmetries much less important. The effectiveness of the LS internal spirals is due not to their mass but either to blockage of the jet where it forms or scatter of jetting condensate downstream.

- Previous calculational studies of energy flow in the nuclear LOS are probably still valid except for cases in which the vapor flow energy is too low to cause substantial pipe expansion ahead of the collapse point. In these, jetting of the steel pipe, which is not included in the calculations, could be important; jetting of stemming material, which occurs in the calculations, could be less important.

- Use of an internal spiral asymmetry on an underground nuclear test is likely to cause a large reduction in condensate jetting (shrapnel) in a test in which LOS vapor flow is held to very low levels - e.g., those seen in Diablo Hawk pre-shot calculations.

The following additional work is recommended in order to improve the level of confidence in any conclusions derived from these studies:

- Repetition of the LS Standard case with various steel pipe wall thicknesses to test the hypothesis that the target damage increases with the wall mass.

- Experiments designed to give better understanding of the mechanism by which the internal spiral prevents damage to the target. For example: a well-diagnosed repeat of the experiment, and also an experiment using symmetric internal rings instead of spirals, to determine whether the spiral works by continuously blocking jetting at the source or by scattering jetting condensate. If rings work well, the latter is indicated.

- Well-diagnosed repeats of the Lead Wrap experiment to gain better understanding of the phenomena. This would also address the reproducibility of the results.

- A heavy Lead Wrap experiment under conditions more like those at the extension in a nuclear test to better determine the relevance of the Lead Wrap results to LOS design. This would imply: the lead wrap would be substantially shorter than the full pipe length; the wall material should vaporize more completely on collapse (perhaps Pb wall at the source end of this and for a comparative "Standard" test); and injection of some energetic vapor at the source. Calculational guidance would be needed.

- Better determination of the statistical variation of other key symmetric experiments, especially the Pinex with heavy pipe and the Standoff configurations, in addition to Lead

Wrap. The spread of the "Standard" results clouds the conclusions of the symmetric cases, particularly the role of the liner and pipe wall - but not the general qualitative conclusions about the asymmetric cases.

- A limited number of calculations zoned finely enough to resolve condensate jetting from the liner would be extremely useful, especially for the Lead Wrap and Standard cases.

SECTION 6
SRII GROUT SPHERE PROGRAM CONTRIBUTIONS

The following section will discuss two aspects of this work. A large body of experimental data has been accumulated. Several aspects of this collection have been analyzed.

6.1 ANALYSIS OF EXPERIMENTAL DATA

The conclusions of this work include the suggestion that powerful confirmation of a rapid stress relaxation exists in the data, and, perhaps, this is related to fluid diffusion as suggested earlier. In addition, the pressurization as observed does not correspond to that expected if the nominal model of events is correct. We believe that there is strong evidence in essentially all the tests that cavity gas leakage through diffusion or some crack flow process plays a significant role before cavity failure. Finally, the LD2C4 experiments indicate an extremely rapid gas and liquid loss, and probably a very fast residual stress relaxation. This characteristic of LD2C4 should be considered in any use of it in investigations of residual stress phenomenology.

6.1.1 Comparison of 2C4 Pressurizations and Residual Stress Relaxation

The data used in this analysis comes from a number of SRII reports. The best summaries of the data are found in recent annual reports, (References 20, 21, and 22). The reader will note that English units are used throughout this section simply because such units are routinely used in the original work, and it appeared that more confusion than enlightenment would accompany a change of units at this time.

The comment has been made by several observers that there seems to be a relation in unvented 2C4 grout pressurizations between an early pressure minimum and the time and amplitude of subsequent fracture.

Table 6.1 summarizes values of pressure and volume scaled from seven presumably identical exploded 2C4 grout cases and five related experiments involving interfaces, faults or tunnels in which the perturbation apparently had no significant effect on the subsequent grout fracture. In every case a 3/8 gm explosive charge was used. The confining pressure was 1000 psi, and water was the hydrofrac fluid. The time of cavity fracture was calculated from the known pumping rate of 4.26 cc/min and an assumption of a 1 or 2 sec delay in the start of pressurization. Available information is somewhat ambiguous on the magnitude of this delay. In some cases it seems to be as long as 6 sec in others 1 or 2 sec. The shortest time will be used in the absence of information to the contrary. This uncertainty is not important for the conclusions to be drawn subsequently.

The first interesting feature is the obvious variation in minimum cavity pressure and volume shown in Figure 6.1. The line is the hyperbola pv = const. There seems to be large scatter at low pressure, but the curve goes close to the average volume for the three lowest points. This looks like an isothermal ideal gas result, but v is the volume of fluid injected into the cavity. It is not the cavity volume itself. In fact, if the cavity volume is assumed to be the same for all tests, and all of the explosive is assumed to react each time, large pressure goes with large unfilled or residual volume. That's a peculiar result.

Since the experiments are nominally identical, it is interesting to speculate on the cause of the variation. Most likely, in our view, is a scatter in cavity size caused by detonator variability. Alternatively, the apparent cavity size changeability could be caused by a variation in grout strength or in void content. A variation in minimum cavity pressure could also indicate some prompt leakage of explosive products. Finally, other so far unidentified causes may exist.

Table 6.1 Selected Data from 2C4 Unvented Grout Sphere Pressurizations.

Shot Number	P_{min} (psi)	V_{min} (cc)	P_{frac} (psi)	V_{frac} (cc)	t_{frac} (sec)
158	1080	.8	3120	6.0	87
159	1080	.8	3040	5.6	81
169	1200	.6	3500	5.4	77
170	1430	.5	3500	4.15	59
199	1000?	?	3100	5.8	83
200	1250	.6	3370	6.0	86
204	1120	.3	3900	4.95	71
*185	1650	.4	4100	4.3	62
*188	1460	.5	3500	4.0	57
*205	1250	.4	3850	6.2	88
*208	1600	.5	3800	4.0	57
*210	1850	.4	4700	4.2	60

* These tests included perturbations such as impedance discontinuities, faults, or tunnels which apparently did not influence the pressurizations significantly.

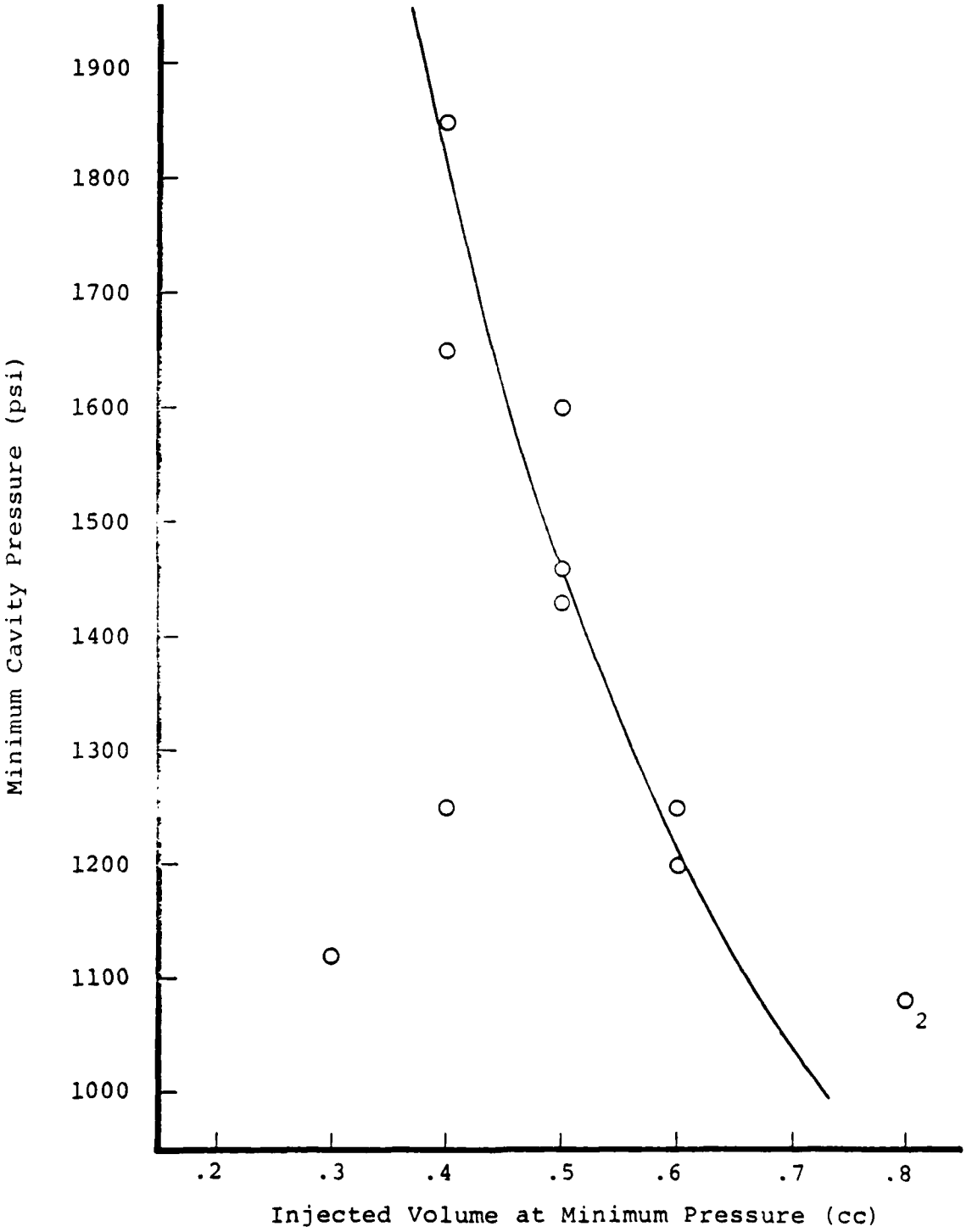

Figure 6.1 Pressure-injected volume relation at first minimum for 2C4 grout spheres.

In addition to the relationship shown in the first figure, Figure 6.2 clearly shows that a correlation exists between the minimum cavity pressure and the fracture initiation pressure. Note that the five experiments involving faults, interfaces, or tunnels seem to give results quite consistent with the others. Two possible correlation lines suggest themselves; one through the origin and one aimed at the 1820 psi value associated with an unexploded cavity. The data agrees equally well with either line, and best with one of intermediate slope. The implications of this relation are not clear at the present time.

A much more interesting correlation is shown in Figure 6.3. There, the time to fracture is plotted against the fracture initiation pressure. There is a considerable scatter in the data, but, clearly, the slope indicates a decreasing fracture initiation pressure with increasing time. Such a decrease has been predicted. The solid line, an eyeball fit to the data, is plotted in Figure 6.4 which is an earlier summary of SRII data which did not contain as much information in the 60-90 second interval. It is interesting to note the excellent qualitative support for the relaxation postulated at that time.*

---

* An aside: Figure 6.4 shows that the pressure required to break unexploded spheres depends on the hydrofracture fluid. Glycerol requires a higher pressure than water. The situation is different for exploded cases. Within the scatter of the data it is difficult to see any difference of significance. In addition, in the long-term creep tests glycerol caused fracture at pressure comparable to those needed for water in the unexploded case. We suggest that the explanation lies in water diffusion driven by the residual stress field.

As the diffusion process proceeds water fills all microcracks near the cavity and may provide a water film over the cavity surface. As a result, subsequent pressurization with a fluid other than water will simply push on the water already present in the critical places. In other words, all exploded sphere fractures are water driven no matter what hydrofrac fluid is used. Gas, water and glycerol should all give essentially the same answers. In addition, the fact that tne pressure required to fracture an exploded sphere with glycerol after many hours is almost the same as that for an unexploded sphere with water is further argument that the residual stress field no longer exists as an effective containment mechanism.

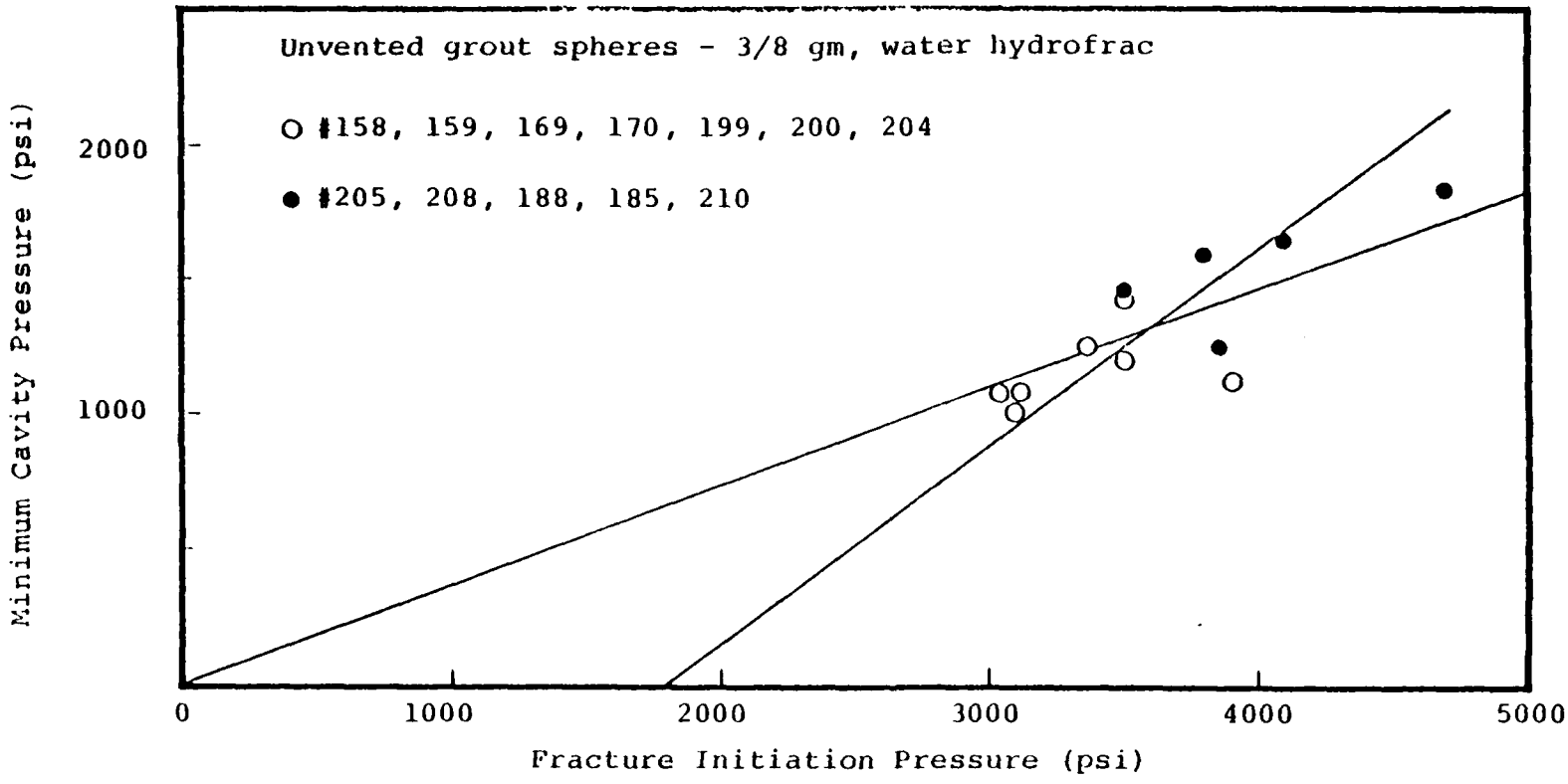

Figure 6.2 Relation between minimum cavity pressure and fracture initiation pressure. The experiments indicated with ● all contained faults, interfaces or tunnels.

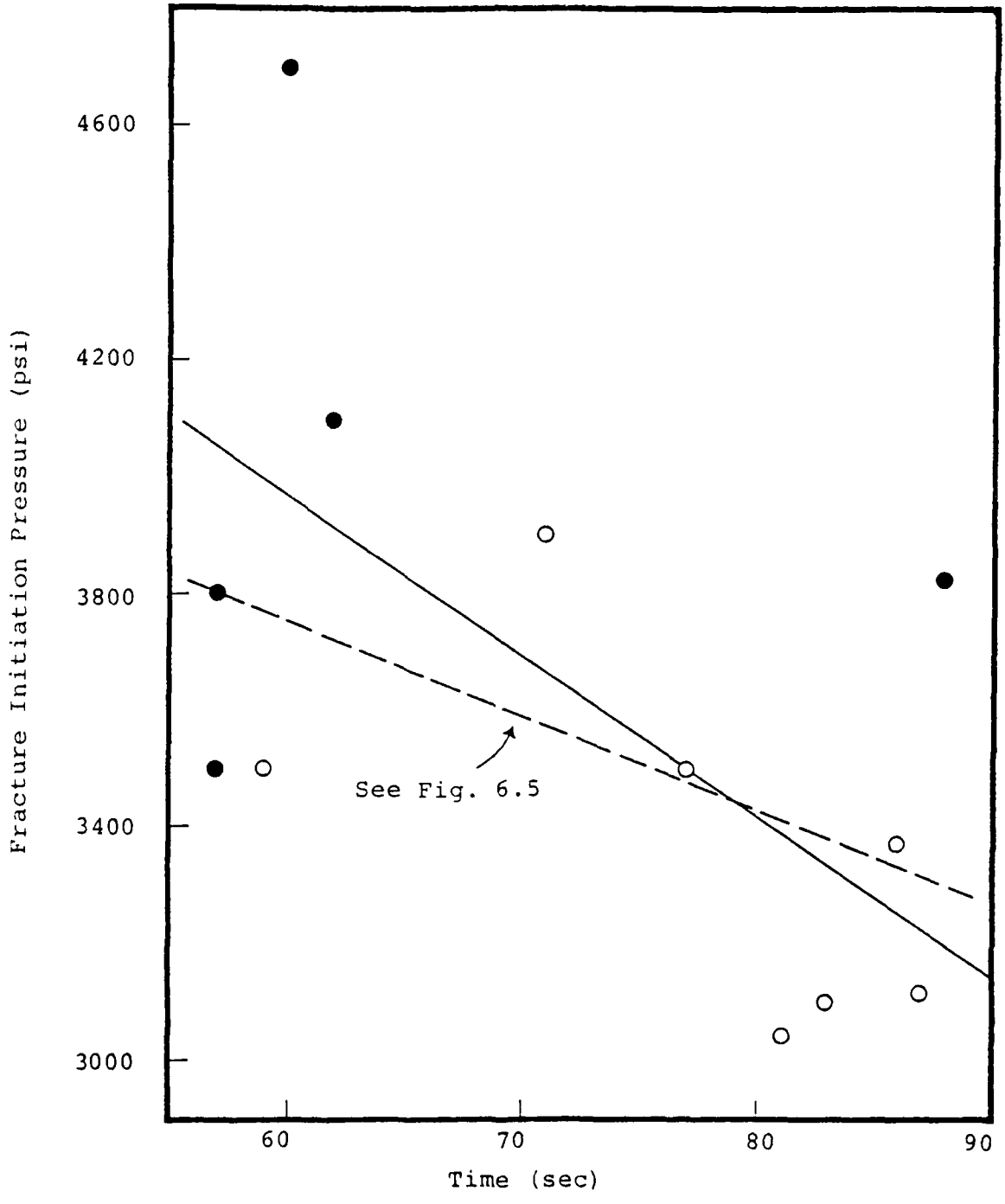

Figure 6.3 Fracture initiation pressure as a function of fracture time for 2C4 unvented grout spheres.

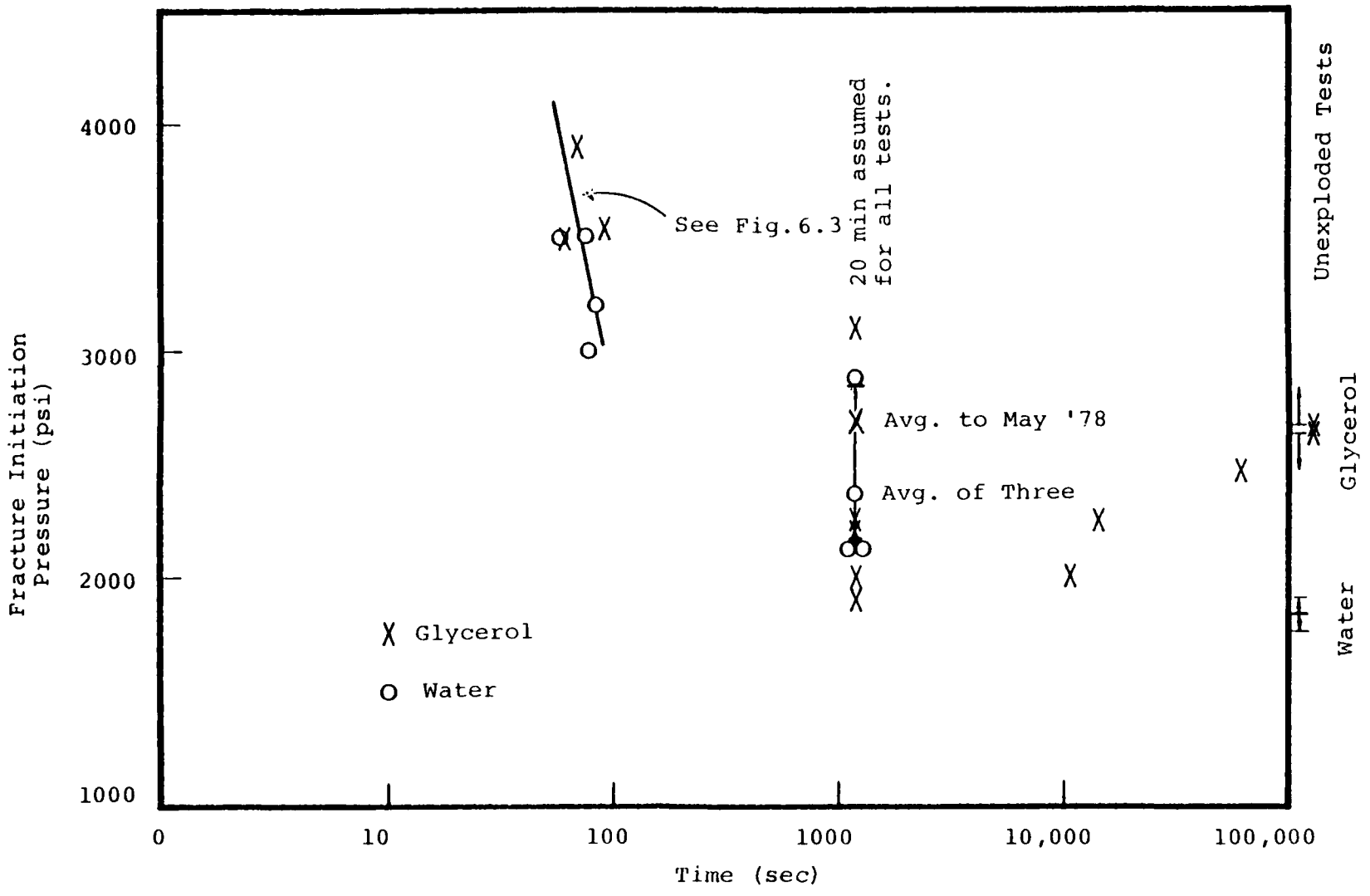

Figure 6.4 Grout spheres hydrofrac data summary.

In a verbal presentation of some of our work Peterson presented a figure in which our predicted diffusive relaxation and the experimental data were plotted together. This figure appears as Figure 6.5, but now the calculated decay has been extrapolated through the experimental data. The slope through the region of the unvented spherical tests is replotted in Figure 6.3 as the dotted line. Note that it agrees with the data about as well as the initial line if the single data point at 60 sec and 4700 psi is considered an outlier and is ignored. The agreement between theoretical prediction and this interpretation of several experiments is surprisingly good. One probably could say the agreement represents a fantastic coincidence because material properties, in particular, the permeability of the shocked and compressed material, are not well known. Nevertheless, these data provide more evidence, probably the best evidence that we now have, that stress relaxation does occur in 2C4 grout. It occurs very rapidly, and perhaps a diffusion process driven by residual stress gradients quantitatively explains that relaxation.

6.1.2 Cavity Filling

Late time cavity pressure was measured in experiments 135 and 142. K. Lie analyzed the heat transfer processes in a caviy and obtained excellent agreement between the experimental data and predictions. In this work the cavity gas was considered to be ideal. Much of the lucite present was assumed pyrolyzed, and the post-shot measured cavity diameter was assumed to apply at early times. The agreement between theory with two values of cavity initial conditions and experiment is shown in Figure 6.6. This work clearly shows that the early cavity pressure response can be explained by thermal conduction mechanisms.

An alternative calculation also explains the pressure decay. If water diffuses into the cavity driven by the residual stress field, it will prevent effective thermal conduction by a process of transpiration cooling while it cools the cavity gas and lowers the cavity pressure.

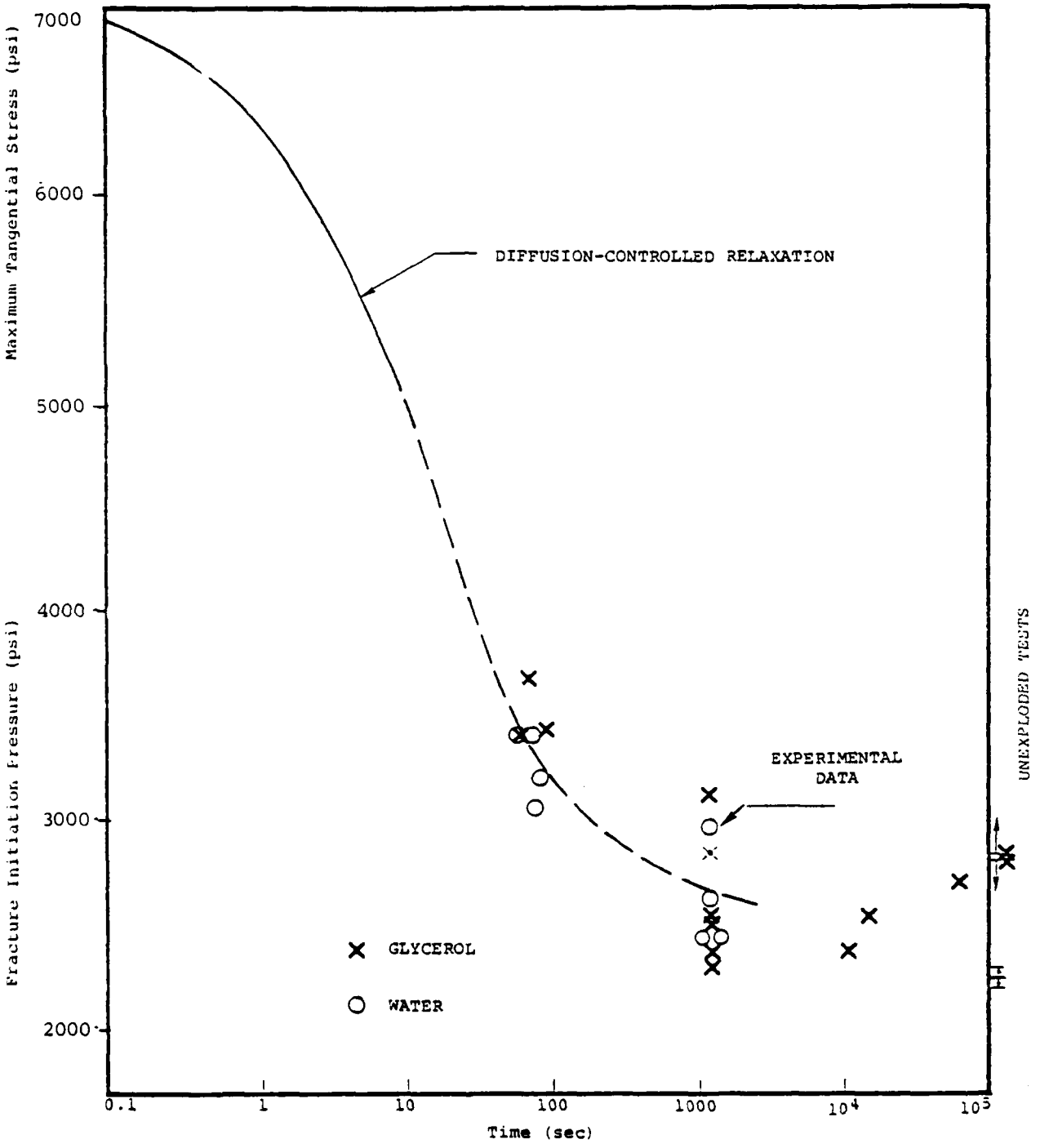

Figure 6.5 Calculated residual stress relaxation as a function of time and fracture initiation pressure for 2C4 grout spheres.

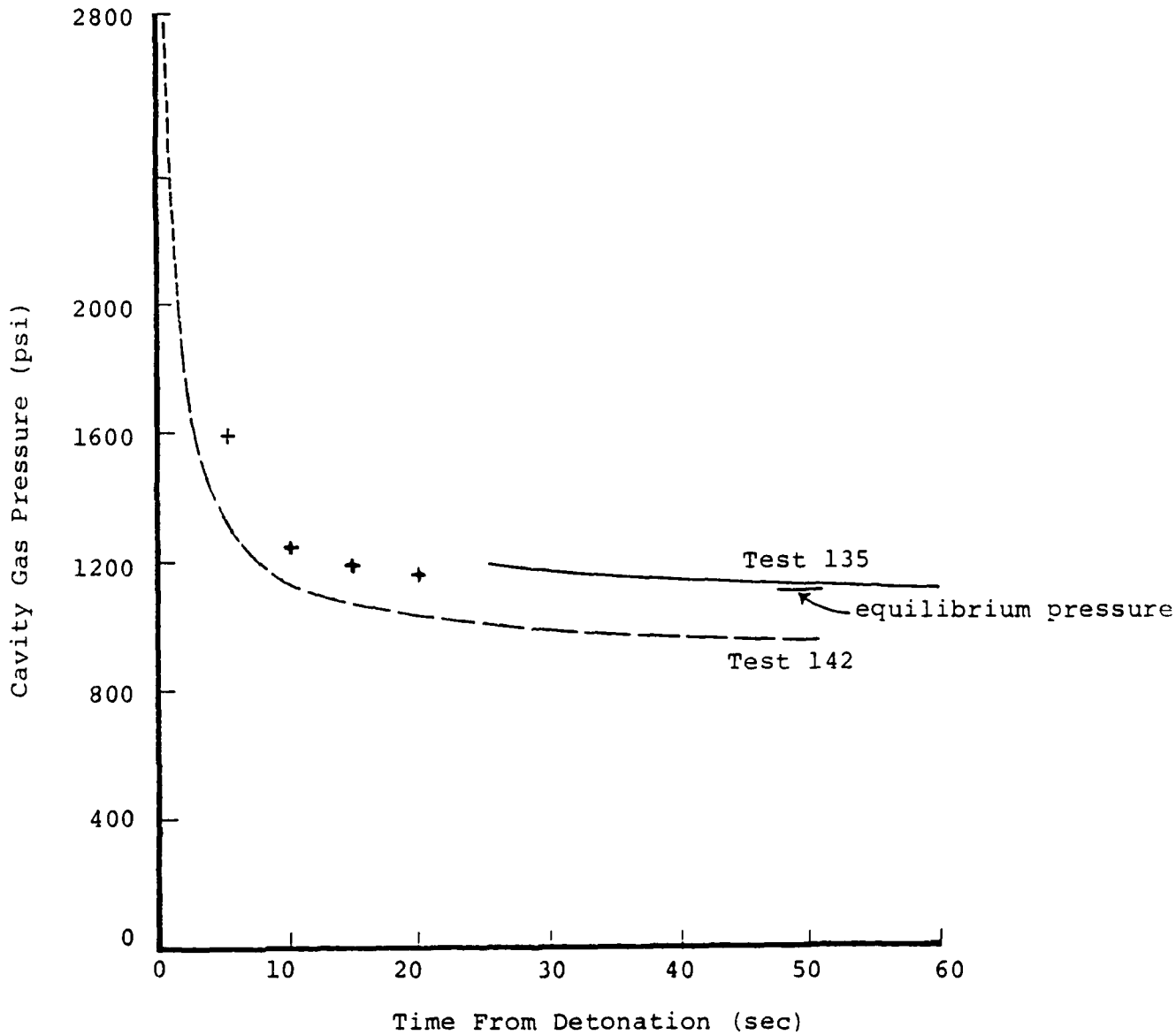

Figure 6.6 Calculated and measured pressure decay in exploded grout sphere.

Figure 6.7 shows the calculated cavity pressure as a function of time compared with the experimental data. In this calculation all water added to the cavity is assumed in thermodynamic equilibrium with the cavity gases present. (The cavity conditions and stress field assumed in this and the previous heat conduction calculation are not consistent with the most recent calculated values.)

Recently, we have tried to consider in more detail the subsequent phases of the pressurization process. In the course of this endeavor new values for cavity volume and moles of cavity gas were computed and the non-ideal gas equation of state was developed for cavity gases. In addition, the influence of elastic expansion of the explosive cavity and fluid compressibility were investigated. The nominal cavity radius is 0.95 cm for 3/8 gm PETN charges detonated in 2C4 grout spheres. This leads to a cavity volume of 3.59 cc. This value should be corrected for several factors tabulated below.

Nominal cavity volume	3.59 cc
Volume of condensed water and carbon from pyrolyzed lucite. .	.14
Volume of det wires, insulation and epoxy	.01
Volume of ball valve in cavity. .	.24
	3.20 cc

The molecular formula for PETN is $C_5H_8N_4O_{12}$. It decomposes as follows:

$$C_5H_8N_4O_{12} \rightarrow 2N_2 + 2CO + 3CO_2 + 4H_2O$$

At conditions of the experiment the water will condense leaving 7 moles of gas per initial mole of PETN.

The lucite probably pyrolyzes to similar products.

$$\text{Lucite,} \quad C_5H_8O_2 \rightarrow CO + H_2 + CH_4 + 3C + H_2O.$$

The carbon and water are condensed. The remainder is gaseous. The total gas mass is 0.0081 moles from the PETN and 0.0039 moles from lucite making a total of 0.012 moles.

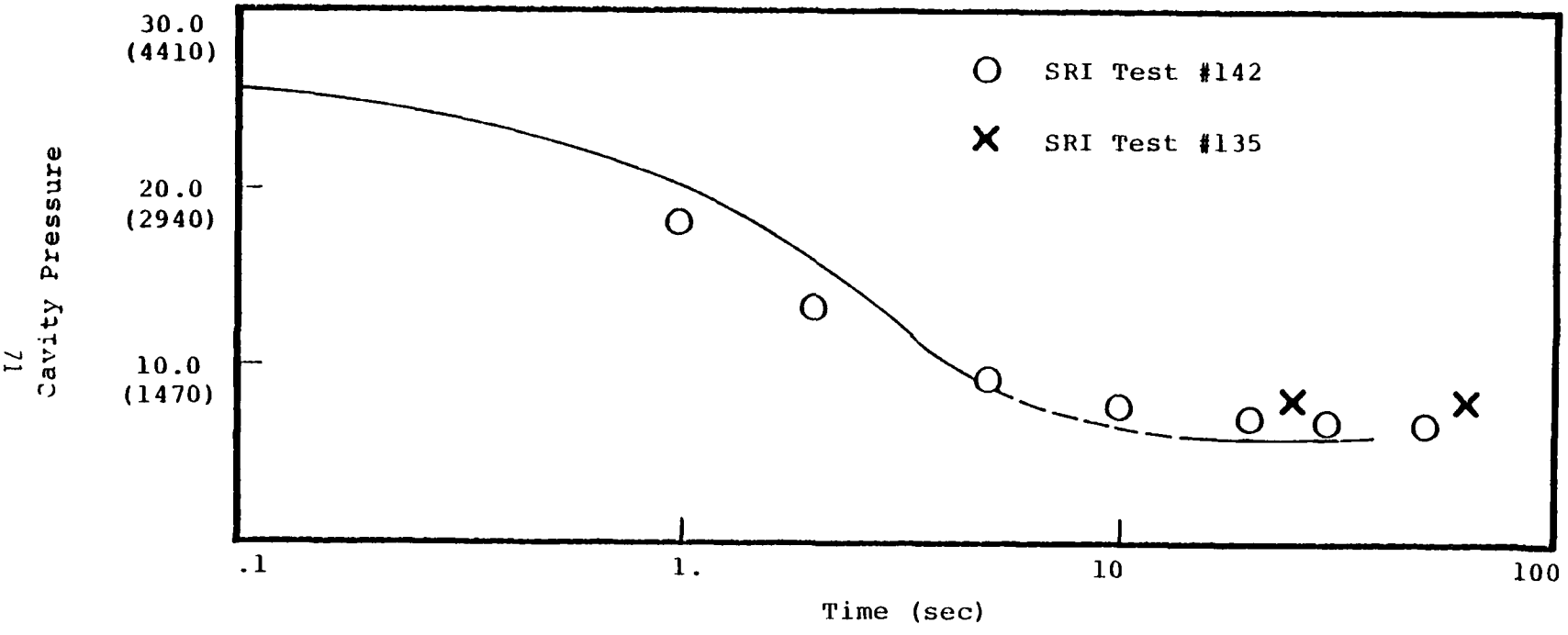

Figure 6.7 Grout sphere cavity pressure decay resulting from water intrusion

The virial gas equation of state will be used to estimate the P-V relationship.

$$PV = nRT\ (1 + BP + \ldots),$$

where

$B_p = \frac{B_v}{RT}$ and $B_v = b - \frac{a}{RT}$, where a and b are Van der Waals constants. Fortunately, b for all components present is close to 0.04. On the other hand, a values vary from 0.25 for H_2 to 3.59 for CO_2. The mixture rules for non-ideal gases are not well established. The usual procedure for a binary mixture gives

$$a_m = a_1x_1 \quad + a_2x_2 \quad + 2a_{12}x_1x_2$$

where a_1, a_2, are a constants for components 1 and 2, respectively. $a_{12} = \sqrt{a_1a_2}$, and x_1 and x_2 are the corresponding mole fractions. This rule was used repetitively to obtain

$$a_m = 1.92\ (l/m)^2\ atm$$

This value cannot be defended vigorously.

The resulting virial coefficient evaluated at ambient temperature is

$$B = -0.0016\ atm^{-1}$$

Note that $B < 0$. This means that the non-ideal gas pressure is less than the ideal gas value at a given v and T. The attractive term, a, dominates the repulsive correction, b, at the low temperatures of interest here.

This analysis leads to a cavity equilibrium pressure at ambient temperature of

$$P = \frac{RT}{\frac{V}{n} + 0.0016RT} = 80.0 \text{ atm} = 1176 \text{ psi}$$

This value is about 20 percent higher than that observed earlier, but it seems consistent with the trend of test 170. On the other hand, if one assumes the lucite does not react, the cavity pressure is only 56.9 atm = 836 psi. This value is too low. Perfect agreement between the calculated pressure and either of the measured values could be obtained by assuming partial lucite pyrolysis. Such a further exercise isn't worth doing because the EOS is also uncertain. (The calculation summarized in Figure 6.6 assumed about 70 percent of the lucite reacted, and gas nonideality was ignored.)

Experiments 169 and 170 were assumed to be representative of unvented 2C4 tests using 3/8 gm charges and water as a hydrofracture fluid. Test 169 was chosen because its fracture initiation as a function of time fits in the middle of the data set, and 170 was used as one of the reference curves by SRII. These curves have been replotted in Figure 6.8. The accuracy is somewhat limited because the curves were scaled from SRII reports and sketched by hand.

The experimental apparatus used to pressurize these spheres has a significant compliance. Figure 6.9 shows the pressurization record for a sealed system. The important point is that the compliance of the apparatus is 3400 psi/cc for pressures greater than about 500 psi. The unvented grout sphere experiments are prepressurized to the order of 500 psi before the experiment begins. Therefore, the relatively large, low pressure initial compliance has already been removed before the experiment begins. Compliance corrected experimental records 169 and 170 are also shown in Figure 6.8. Note that for 169 the apparent fracture volume exceeds the nominal cavity volume.

As a sphere is pressurized, an elastic response occurs in the surrounding grout. The radial distortion associated with this elastic response follows from the equation

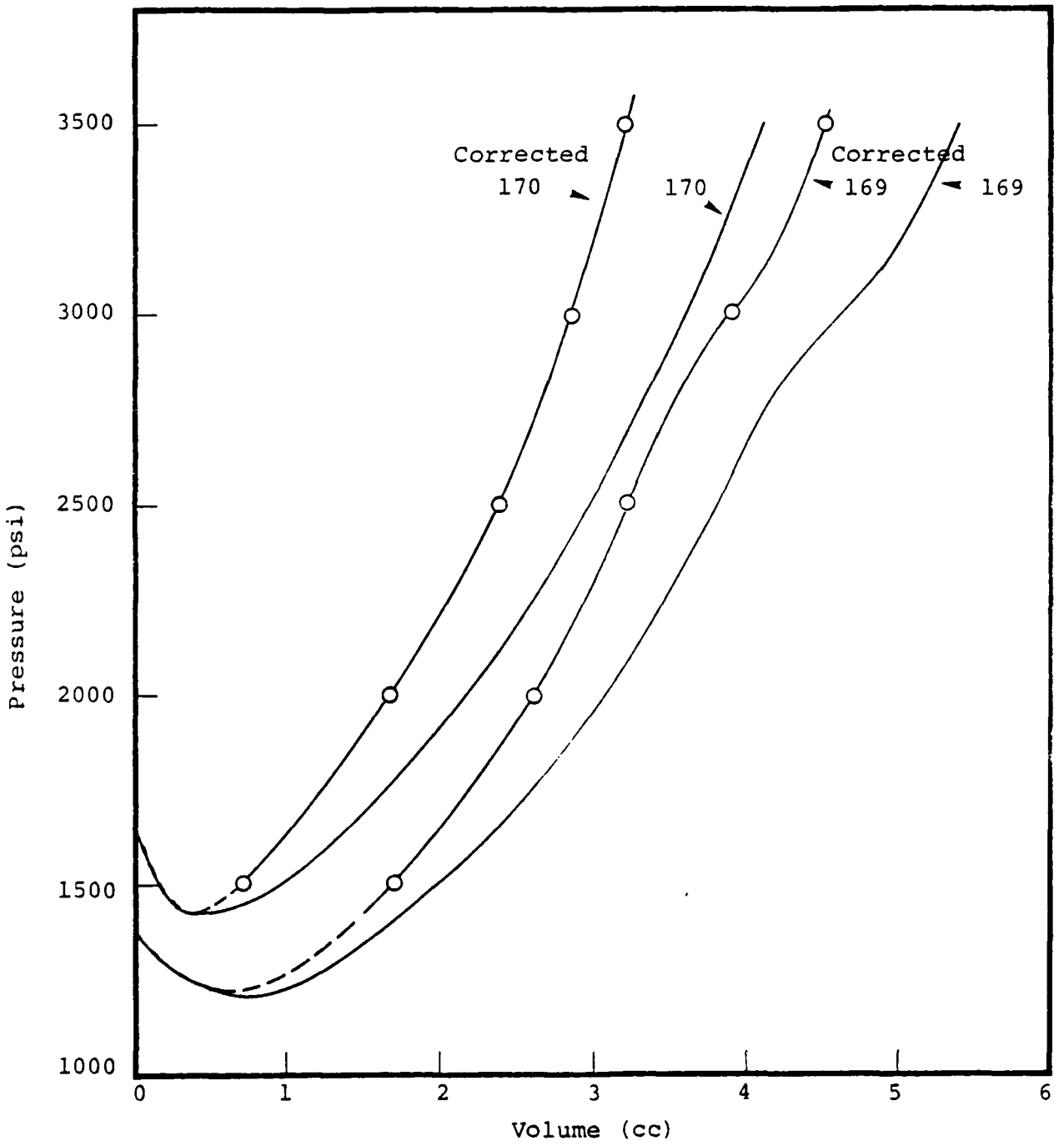

Figure 6.8 Original and compliance-corrected pressurization records for tests 169 and 170.

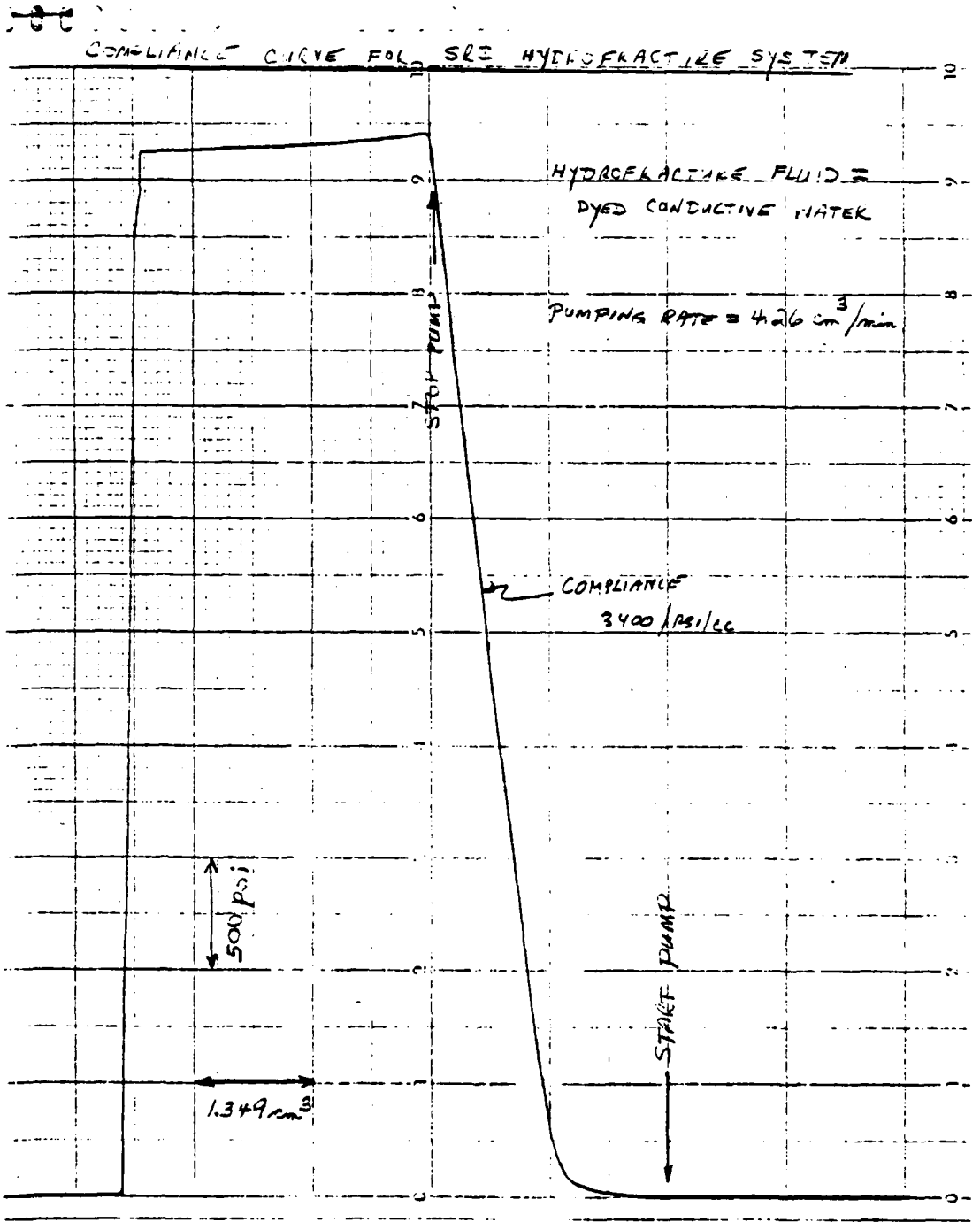

Figure 6.9 Compliance curve for SRII hydrofracture system.
[This figure is taken from J.C. Cizek, Reference 23.]

$$u_a = \frac{a}{E}\left\{P_i\left[\nu + \frac{1+\frac{2a^3}{b^3}}{2\left(1-\frac{a^3}{b^3}\right)}\right] - \frac{3P_o}{2\left(1-\frac{a^3}{b^3}\right)}\right\}$$

where a and b are inner and outer radii. P_i and P_o are inner and outer pressures, ν is Poisson's ratio and E is Young's modulus. For E = 176 kb and ν = .295 the elastic distortion leads to a volume change of a few times 10^{-3} cc, this is very small compared to fluid volumes and is negligible.

It is also straightforward to investigate the compressibility of water in the cavity. The handbook value for this compressibility is roughly 40 $Mbars^{-1}$. This leads to a volume change of approximately 1 percent at 3500 psi. A 1 percent correction to the volume at the highest pressure of interest is quite negligible compared to other uncertainties.

On the basis of these factors the cavity pressurization to be expected has been calculated assuming the cavity starts from a thermal equilibrium state which is reached experimentally after 10 to 15 seconds (see Figure 6.6) and the subsequent pressurization is assumed to be an isothermal process. This also seems to be an excellent approximation. The virial EOS was used. Table 6.2 lists the volume of cavity gas and the volume of liquid to be expected in the cavity at a number of pressures between 1500 and 3500 psi.

TABLE 6.2

Calculated pressure-volume relationship for unvented 2C4 grout sphere tests. The cavity volume was assumed to be 3.2 cc, 0.0120 moles of gas were assumed present, the cavity was assumed isothermal, and the virial gas law was used.

P (psi)	V_{gas} (cc)	V_{liquid} (cc)
1176	3.20	0
1500	2.41	0.79
2000	1.69	1.51
2500	1.26	1.94
3000	0.96	2.24
3500	0.77	2.43

The calculated pressurization is shown in Figure 6.10 together with the experimental data. The agreement between experimental results from test 170 and the prediction is good at early time, but at late times the pressure observed experimentally is too low, or, correspondingly, too much fluid must be injected into the cavity to develop a given pressure. The agreement with 169 is not very good. Note that the volume of fluid required exceeds the measured cavity volume. We believe that the disagreement between experimental and theoretical results indicates that some leakage of cavity gas occurs. This may be diffusive or related to a developing crack system. The analogy with late time cavity pressure development as presented by Peterson and Lie (Reference 2) is certainly thought provoking.

The volume of fluid required for test 169 exceeds cavity volume, but there is no clear indication of a change in slope which would indicate a point of cavity fill. On the other hand, test 159 shows a break which might be so interpreted at a volume of 5 cc and a pressure of 2500 psi. The volume even after correction for compliance exceeds cavity volume. This suggests that either the variability in initial cavity volume is larger than reported by SRII or the early leakage involves fluid as well as gas.

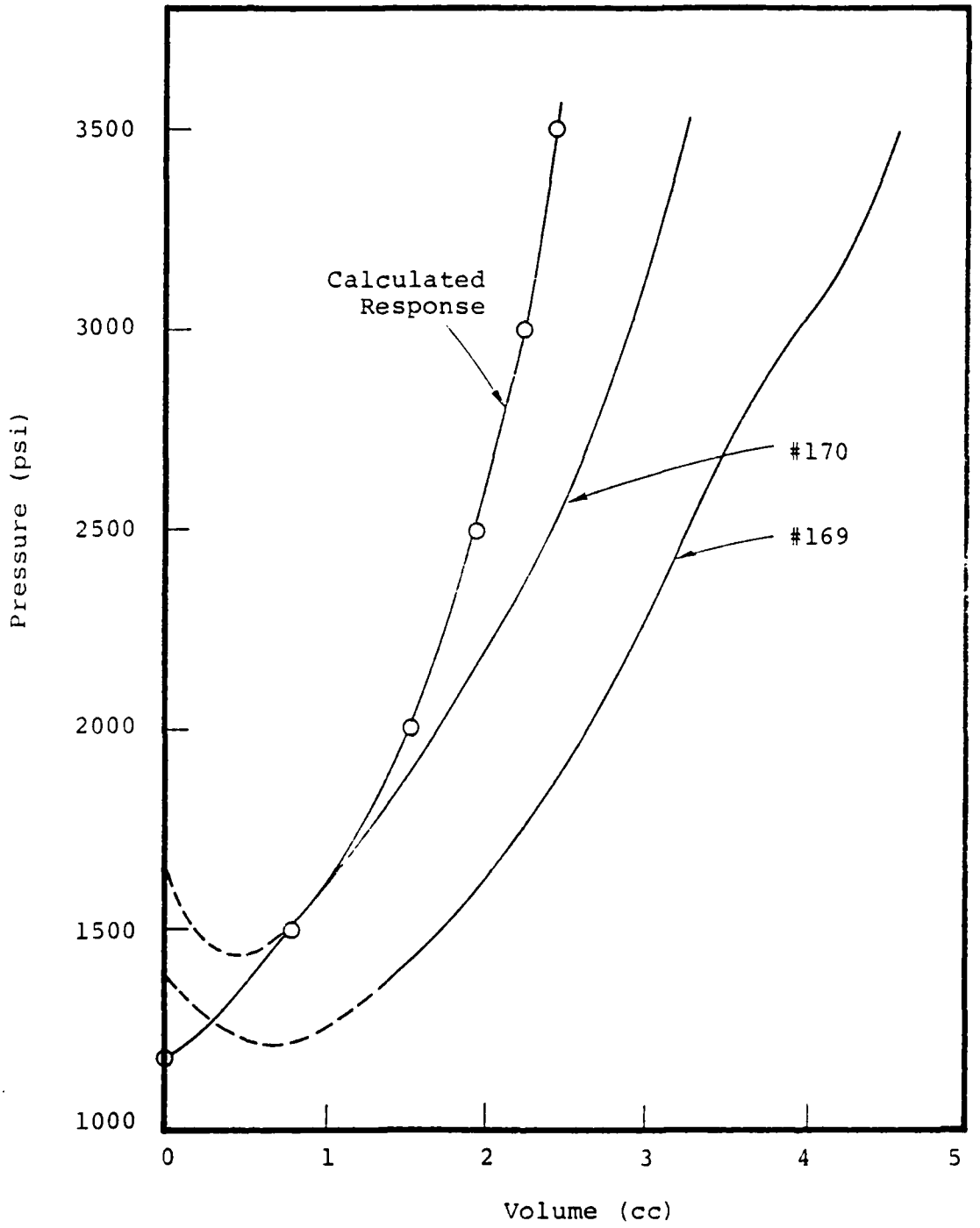

Figure 6.10 Comparison of compliance corrected and calculated pressurization records for unvented 2C4 grout spheres.

6.1.3 LD2C4 Experiments

For the LD2C4 experiments, 189, 215, and 216 reported in the November, 1979, bimonthly from SRII and reproduced in Figure 6.11 no compliance correction is required up to the point of the very conspicuous break in pressurization slope at roughly 7 cc volume. This follows because the break occurs at a pressure of the order of 500 psi which is approximately the preshot pressurization level of the system.

Note that test 189 shows a steady pressure decrease while the pressurization process proceeds. This suggests that a major leak or diffusion process is underway. Gas is leaking out faster than fluid is being pumped in.

The calculated cavity volume for test 189 is 7.42 cc. The fluid volumes injected at the break from the three nominally identical tests are 7.0, 7.6 and 7.7 cc in excellent agreement with the calculated volume. This then supports the identification of the break as the point in which fluid fills the volume. Subsequently, since the fluid is more viscous than explosive products, its diffusion or leakage from the cavity is less rapid, and pressure increases in the cavity at an increased rate as pressurization proceeds.

A compliance curve drawn at 3400 psi/cc in the vicinity of the steep portions of these curves is also shown in Figure 6.11. Note that in every case the pressure increase is less rapid than the apparatus compliance would suggest. This clearly indicates that significant additional quantities of fluid are being lost from the cavity as the process continues.

The most convenient explanation for the peculiar performance of the LD2C4 material involves the widespread collapse of microspheres in the material. This probably leads to an unusually high permeability. It would be instructive to attempt permeability measurements on small samples of material taken from the vicinity of the cavity.

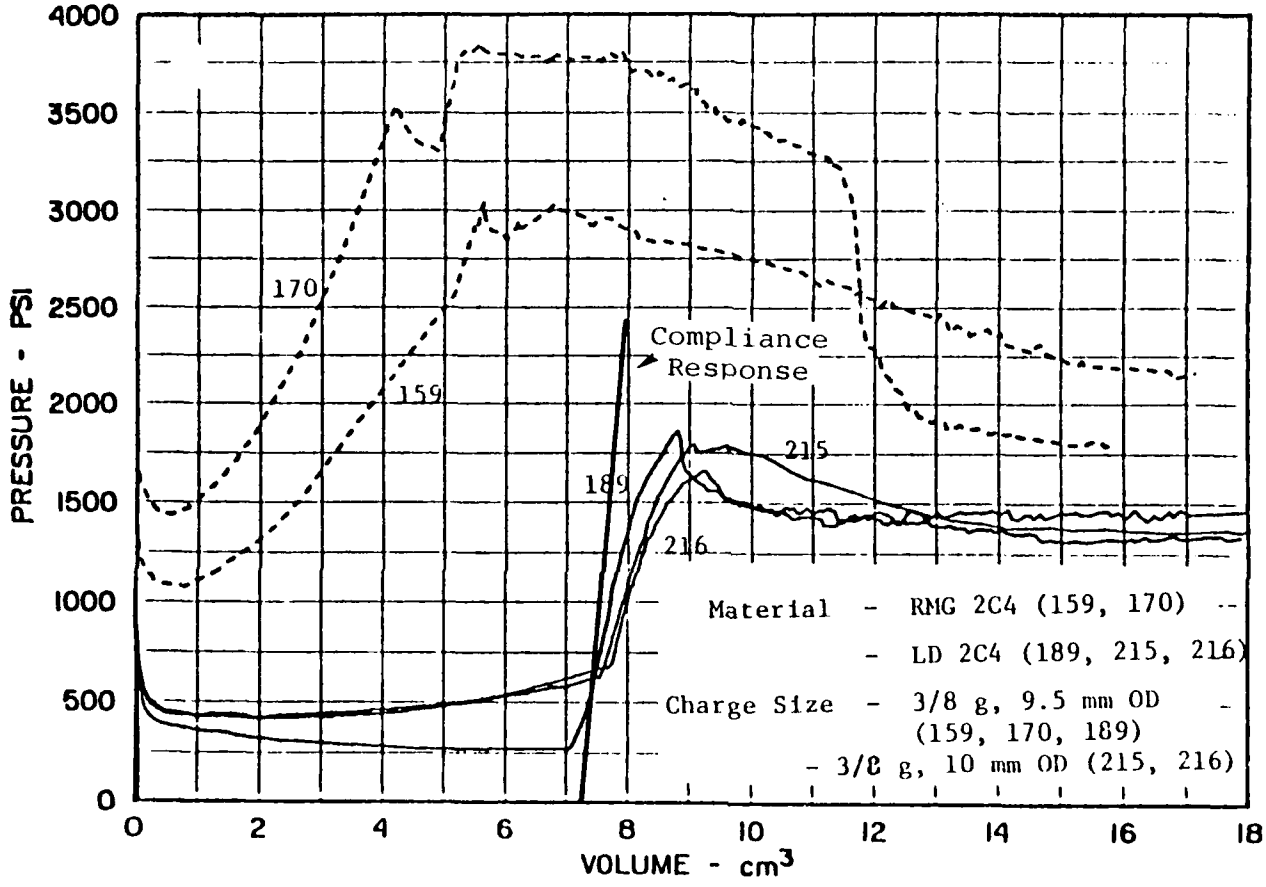

Figure 6.11 Hydrofracture pressures for unvented exploded cavity tests 159, 170, 189, 215, and 216 - material property.

The final fracture initiation pressure indicated by these three records is approximately 1750 psi. This value is essentially identical with the pressure required to fracture an unexploded 2C4 cavity (see Figure 6.4). Insofar as the strengths of the two materials are similar, the conclusion follows that the residual stress field in LD2C4 is gone by the time the fracture begins roughly 2 minutes after the experiment. This is consistent with the apparent very high permeability of this material, and it again provides support for a rapid stress relaxation, possibly related to pore fluid diffusion.

It appears that the LD2C4 is a unique material. Because of its formu'ation from microspheres, the permeability of strongly shocked material appears to be very high, and, therefore, the stress decays at an unusually rapid rate.

6.1.4 Summary

Recent SRII tests have been analyzed from several points of view. The most interesting results seem to provide additional evidence for the very rapid decay of residual stress states and to support the rather general observation of cavity leakage before fracture occurs. The latter point coupled with Peterson's conjecture that some form of leakage may be important in the nuclear case may have real significance to containment when it is understood.

We have emphasized rapid residual stress relaxation in several places in this section. We have speculated that water diffusion driven by the stress field is a major mechanism causing this relaxation. We do not mean to imply that conventional creep may not also play a role, perhaps even a dominant role. On the other hand, the physics involved in the diffusion process seems intuitively attractive, the calculated relaxation rate is very fast, and there are experimental data from grout sphere tests, large HE explosions, and nuclear events to support that mechanism.

6.2 EXPLOSION CALCULATIONS

A calculational study of four laboratory grout sphere configurations has been made by Rimer (Reference 24). This is an extension of work reported earlier by Rimer and Lie (Reference 25) in which calculations were made for the four test configurations; (1) the standard 2C4 sphere, (2) the decoupling shot, (3) the low density rock matching grout (LD2C4) and (4) the granite simulant (GS3). All of the initial calculations gave cavity radii significantly larger than the measured values except for the decoupled shot which gave reasonable agreement. The low-density grout calculation showed the largest cavity radius, the smallest cavity pressure, and the smallest maximum residual hoop stress. The granite simulant calculation gave the smallest cavity but the largest cavity pressure and residual stress. The cavity pressure was greater than 1 Kbar. In all three coupled shots, the maximum residual hoop stress was approximately a factor of two greater than the calculated cavity pressure.

For the decoupled cavity shot the cavity pressure was about a factor of two greater than for the coupled 2C4 test. However, the residual hoop stress for the decoupled cavity test was largest near the cavity and nowhere exceeded the cavity pressure, not an ideal situation for containment. In spite of this, the measured hydrofracture pressures for the decoupled tests were essentially the same as for the coupled 2C4 experiments. This seems to reinforce the hypothesis that the residual stresses have relaxed with time. However, another possibility exists. Rimer and Friedman (Reference 26) have reported calculations for nuclear events in NTS Area 12 tuff in which the results for coupled and decoupled events are qualitatively similar to the results presented here. These calculations also showed that when the cavity pressure is allowed to decay to zero, the peak residual hoop stresses for the coupled and decoupled cases are very similar and only slightly smaller than for the coupled case before pressure decay.

One disturbing aspect of these initial calculations is the large cavity radii (27 percent greater than the measurements for the standard 2C4 sphere). A careful examination was made of the physical dimensions of the experiment including charge weight and density, thickness of lucite shell around the explosive, location of charge relative to the quartz gauge, and material properties of the 2C4 grout. As a result, the calculational model described in Reference 25 was altered; the major changes being a reduction in weight of PETN from the nominal 0.375 g to 0.360 g, using slightly more lucite, a somewhat different failure envelope for low pressures, and a new location for the quartz gauge at a radius of 16.8 cm instead of at 17.8 cm. The calculated cavity radius decreased only about 2 percent as a result of these changes.

The effect of moving the assumed location of the quartz gage closer in was to increase the calculated impulse by 42 percent, making it approximately 20 percent greater than the largest reported value and 30 percent greater than the average of the three reported values. Cizek (Reference 23) estimates that the gage is located at 16.8 cm within a tolerance of $\pm$ 3 to 6 mm. Based on our calculations, this means that the possible error in impulse due to locating the gage alone may be as great as 15 to 30 percent, irrespective of the reproducibility of the PETN detonation process.

SRII has recently performed mechanical properties tests on the three materials of interest, 2C4, LD2C4, and GS3. Tests were conducted of uniaxial compressive strength and splitting tensile strength under both static and dynamic (strain rate of 0.15 or 0.25 sec^{-1}) loading. For all three materials, the tests under dynamic loading conditions showed significantly higher compressive strengths (30 to 60 percent) and tensile strengths (60 to 80 percent).

Our calculations showed strain rates as large as 2×10^5 sec^{-1} in the sphere of 2C4 grout, several orders of magnitude greater than would be expected in a prototype nuclear or HE event at the same

stress levels. The laboratory mechanical properties tests suggest that the grout sphere results cannot be scaled to the large length scales of interest in the nuclear case because of their large strain rates. Our constitutive strength models were changed to take account of the increase in strength of the spheres under higher strain rate loading. This required extrapolating the laboratory strain rate data to the considerably larger strain rates of interest. This extrapolation was based on an assumed linear relation between strength parameters and the log of the strain rate. Calculations made using this crude dynamic strength model gave cavity radii within 5 percent of the data for all cases except the low-density grout (LD2C4) in which the calculated cavity radius was low by approximately 10 percent.

The larger strengths implied by the dynamic strength model resulted in a significantly narrower positive overpressure pulse at the quartz gauge than obtained with the original strength model and thus a smaller impulse. The peak pressures were basically the same. Quartz gauge data are available only for the standard 2C4 grout tests and the low density LD2C4 tests. In these cases, the measured durations of positive overpressure were in far better agreement with the calculations using the dynamic strength model than the static strength model. All calculated peak pressures were lower than the data. The calculations using the static strength model gave impulse at the gages larger than the average data by approximately 10 to 30 percent, but for the dynamic strength model the impulse was smaller than the data by 30 percent for 2C4 but in good agreement for LD2C4. Since the possible error in impulse due to locating the gage to within 3 to 6 mm is calculated to be 15 to 30 percent, we feel that too few measurements have been made to evaluate our calculations in terms of impulse.

In summary, the calculations have demonstrated that a higher strength than given by the static laboratory measurements may be needed to match the cavity radius data. Our crude model based on the measured dynamic strengths gives a reasonable match to these data. The higher strength results in larger cavity pressures and higher peak residual

stresses. These calculated values are even less consistent with the hydrofracture pressure records unless some time dependent creep or stress relaxation explanation is invoked. This serves to confirm the need for experimental hydrofracture data made on a significantly shorter time scale.

SECTION 7
MISCELLANEOUS TASKS

During the course of this contract, a number of relatively minor activities were undertaken. They will be briefly summarized below.

7.1 CEP SUPPORT

One member of the S^3 staff has been asked to serve as a consultant on the Department of Energy Containment Evaluation Panel. This support to the CEP has required a small but continuing level of effort.

7.2 SLIFER STUDIES

It was mentioned during the Mighty Epic containment summary report discussion that slifer records obtained in the vicinity of the muffler showed peculiar discontinuities which could not be immediately explained. An effort was made to analyze these discontinuities under the following assumed scenario (Reference 27). The fast plasma flow, which was too weak to crush the slifer, may have been strong enough to damage the slifer in the vicinity of the muffler as this flow interacted with muffler baffles. This damage would modify the slifer impedance in such a way as to introduce a systematic error in the record until the damaged cable was fully crushed by ground shock arrival at the muffler. Presumably, this late-time slifer crush would give rise to a discontinuity as the damaged section was removed from the electrical circuit.

To test this hypothesis a slifer oscillator and length of cable were obtained from Sandia Corporation, a number of experiments were made, and calculations performed of the response characteristics of a slifer system with damaged cable. A number of damage modes were investigated including crushing, stretching, high impedence shorting,

removal of the external shield, etc. In no case was a credible perturbation to the slifer identified which would explain the discontinuities observed in the Mighty Epic slifer records. In fact, the most credible perturbation, a partial crushing or squeezing of the cable, caused an impedance change of opposite sign to that required to explain the observations.

7.3 SWIS CODE DEVELOPMENTS

The SWIS code which has been used for grout sphere investigations has been modified extensively by several workers over the course of the last few years. An improved version of the code has been prepared which incorporates desirable features of several of these modifications, improves calculation efficiency, and eliminates unnecessary calculational baggage which had accumulated through time. The revised code is significantly more efficient and convenient to use, and internal code documentation has been provided.

7.4 STREAK/UNION CODE IMPROVEMENTS

Major improvements have been made in the techniques for calculating energy injection and flow in the LOS. FLIP had previously been employed to calculate LOS flow in the composite UNION code, in which it couples with the 2-D Eulerian STREAK code. A major simplification has been achieved in removing FLIP and allowing STREAK to perform the calculation of the ablation-dominated LOS flow. STREAK now calculates the ablation rate on the basis of local averages of flow quantities over the pipe cross section as FLIP does. The ablation model described in Section 4 is used, with the ablation products instantly spread over the pipe cross section. This approximation has been shown to be adequate for flow in an initially-evacuated LOS and also for the early-time portion of flows into ambient air (in which the flow is source-dominated, not ablation dominated). Comparison tests have shown that this technique gives solutions for LOS flow that are quite consistent with those obtained with FLIP. This technique became possible only after the dev-

elopment of the "two-velocity" representation of mixed cells in STREAK, whereby the LOS vapor and surrounding stemming may have very different velocities in the cell containing their boundary. Another benefit is that this technique allows better modeling of the vapor flow between the collapse point and the tip of the "grout jet" that is often seen in calculations. When FLIP was used it was necessary to limit it to the pipe ahead of the jet.

The technique for injecting vapor across an Eulerian material boundary into the LOS when the solid bounding the LOS becomes sufficiently hot has also become a permanent part of STREAK. (This was intially described in last year's Final Report (Reference 12) in connection with calculations of the PI simulations.) Subsequent 1-D calculations of a shock propagating through a solid and unloading at a free surface have shown that this vaporization model gives results which agree much better with analytic results than those obtained without it. This is expected to give more realistic results near the source than were previously obtained. Note that the physical process is the formation of vapor, say from material in a solid iron extension, by shock or compression heating. This is in addition to any surface ablation which may occur. The latter is provided by the LOS ablation model.

SECTION 8
REFERENCES

1. Bailey, L. E. Jr., and Duff, R. E., "Cavity Venting for Low Yield Test Design", Systems, Science and Software Topical Report SSS-R-80-4342, 1979,

2. Peterson, E. and Lie, K., "Evaluation of Late Time Cavity Pressure", Systems, Science and Software Report SSS-R-80-4310, January 1980.

3. Barthel, J. R., Peyton, S., Pyatt, K. D., and Wu, H. E., "Ablation and Boundary Layer Growth Effects Behind High-Speed Shock Waves in Pipes and Tunnels", Systems, Science and Software Topical Report, to be published in April 1980.

4. Barthel, J. R. and Patch, D. F., "Condensation Modeling in the FLIP Code, Vol. I - Description of the Model", Systems, Science and Software SSS-R-75-2535, January 1975. See also Vol. II - "Application to LOS and Other High Energy Flows", by D. F. Patch and J. Barthel, SSS-R-75-2536, January 1976.

5. Baum, D. W., Gross, M. B. and Gill, S. P., "LOS Pipe Experiments", Physics International Final Report DNA 3036F, February 1973.

6. Barthel, J.R. and Patch, D. F., "FLIP Calculations of Experimental Configurations and of Geometry and Yield Effects", Systems, Science and Software SSS-R-73-1901, September 1973 (also summarized in Final Report DNA 3269F, November 1973).

7. Barthel, J. R., "Comparison of Hybla Fair Cavity, LOS and Ground Motion Calculations with Data", Systems, Science and Software Report SSS-R-75-2607, April 1975.

8. Thomson, J. M., "Marvel Revisited: Experiment Design and Data Analysis", Lawrence Livermore Laboratory, UCRL-52445, February 1978; see also "Marvel Data Reanalysis" by R.E. Duff, included as Appendix in Reference 3 above.

9. Barthel, J. R., "Analysis of Ablation-Dominated LOS Flows Using and Improved Model of Ablation", Systems, Science and Software Topical Report, draft to be released April 1980.

10. Moore, E. T., Jr., and Funston, R., "Asymmetric Collapse of LOS Pipe," Physics International Co. Draft Final Report, PIFR-1034, 20 July 1979.

11. Moore, E. T., Physics International Co., private communication.

12. Duff, R. E., Peterson, E. W. and Barthel, J. R., "Late Time Containment Research", Final Report SSS-R-79-3973, February 1979.

13. Bjork, R. L., "Review of Physical Processes in Hypervelocity Impact and Penetration," Proc. 6th Symposium on Hypervelocity Impact, Vol. II, Part 1, August 1963. (Also appeared as Rand Corp. RM-3529-PR, July 1963).

14. Wagner, M. H., Brooks, N. B. and Bjork, R. L., "Impact of Porous AL Projectile on AL at 20 and 72 km/sec," Proc. 7th Symposium on Hypervelocity Impact, Vol. III (Theory), February 1965.

15. The Hypervelocity Impact Symposium, Vol V (Experiments), February 1965.
    a. Palmer, E. P. and G. H. Turner, "Energy Partitioning in High-Velocity Impact Cratering in Lead".
    b. Halperson, S. M., "Comparison Between Hydrodynamic Theory and Impact Experiments.

16. Birkhoff, MacDougall, Pugh and Taylor, J. of Appl. Phys., 19, p. 563 (1948).

17.. Sedgwick, R. T., Systems, Science and Software: private communication regarding his experience with shaped charge jetting calculations.

18. Jeanloz, R. and Ahrens, T. J., Journal of Geophysical Research, 84, No. B-13, p. 7545, December 10, 1979.

19. Glenn, H. D., Lawrence Livermore Laboratories, private discussion of high speed photography in early simulation experiments.1.

20. Cizek, J.C. and Florence, A. L., "Laboratory Investigation of Containment in Underground Nuclear Tests" SRI International Report SRI PYU-5958, DNA 4846, January 1978.

21. Cizek, J. C. and Florence, A. L., "Laboratory Studies of Containment in Underground Nuclear Tests", SRI International Report SRI PYU-5958, January 1979.

22. Cizek, J. C. and Florence, A. L., "Laboratory Studies of Containment in Underground Nuclear Tests", SRI International Report SRI PYU-8113, January 1980.

23. Cizek, J. C., private communication, August 29, 1979.

24. Rimer, N., "Spherically Symmetric Calculations of the SRI Grout Spheres Experiment for Four Different Laboratory Configurations", Systems, Science and Software Report SSS-R-80-4240.

25. Rimer, N. and Lie, K., "Spherically Symmetric Numerical Simulations of the SRI Grout Spheres Containment Experiments", Systems, Science and Software Topical Report SSS-R-79-3831.

26. Rimer, N. and Friedman, M., "Residual Stress and Coupling from Nuclear Shots in a Cavity", DNA 459 IT, Systems, Science and Software Report SSS-R-78-3596, April 1978.

27. Groethe, M. and Ginn, W., "The Frequency vs Length Response for a Deformed Slifer Cable", Systems, Science and Software Report SSS-R-80-4374, February 1980.

DISTRIBUTION LIST

DEPARTMENT OF DEFENSE

Defense Nuclear Agency
ATTN: SPTD, T. Kennedy
4 cy ATTN: TITL

Defense Technical Information Center
12 cy ATTN: DD

Field Command
Defense Nuclear Agency
ATTN: FCTMD, W. Summa
ATTN: FCTK, C. Keller

Field Command Test Directorate
Test Constructions Division
Defense Nuclear Agency
2 cy ATTN: FCTC, J. Lacomb

DEPARTMENT OF ENERGY CONTRACTORS

Nevada Operations Center
ATTN: R. Newman

Lawrence Livermore National Laboratory
ATTN: D. Oakley
ATTN: B. Hudson
ATTN: B. Terhune
ATTN: J. Shearer

Los Alamos National Scientific Laboratory
ATTN: R. Brownlee
ATTN: E. Jones/F. App
ATTN: A. Davis
ATTN: L. Germain
ATTN: S. Schmidt

Sandia National Laboratories
Livermore Laboratory
ATTN: R. Bass
ATTN: (Div 1111), C. Mehl/C. Smith

OTHER GOVERNMENT AGENCIES

Department of the Interior
U.S. Geological Survey
ATTN: R. Carroll

DEPARTMENT OF DEFENSE CONTRACTORS

California Research & Technology, Inc
ATTN: M. Rosenblatt

Pacifica Technology
ATTN: G. Kent

Physics International
ATTN: E. Moore

SRI International
ATTN: A. Florence

Systems, Science & Software
ATTN: R. Duff

Terra Tek, Inc
ATTN: S. Green

R & D Associates
ATTN: P. Haas

General Electric Company—TEMPO
ATTN: DASIAC


DAT
FILM